Numerical analysis of the performance enhancement of a latent heat storage shell and tube unit using finned tubes during melting and solidification

Mohamed Amine Dekhil, Jules Voguelin Simo Tala, Odin Bulliard-Sauret, Daniel Bougeard

Version of Record: https://www.sciencedirect.com/science/article/pii/S135943112100315X
Manuscript_6b0f50317538b43d552818da2f6f2636

Numerical analysis of the performance enhancement of a latent heat storage shell and tube unit using finned tubes during melting and solidification

Mohamed Amine DEKHIL[1, *], Jules Voguelin SIMO TALA[1], Odin BULLIARD-SAURET[1, 2], Daniel BOUGEARD[1]

[1] IMT Lille Douai-941 Rue Charles Bourseul, 59500 Douai
[2] HEI-Yncrea Hauts-de-France, 13 Rue de Toul, 59000 Lille
[*](Corresponding author: mohamed-amine.dekhil@imt-lille-douai.fr)

Abstract

The present study deals with the numerical analysis of the melting and solidification processes in three horizontal storage units for Latent Heat Thermal Storage (LHTS) using water, around its density-temperature inversion point as phase change material (PCM) and a water/glycol solution as the Heat Transfer Fluid (HTF). One of these storage units, made of a plain tube and a shell is used in this study as the reference against which the other two configurations, made respectively of longitudinal and radial finned tube and shell are compared at constant heat transfer surface, compactness and PCM volume. The objective is to improve the thermal performance of the reference unit, and therefore the charge and discharge rates using surface extension. The effect of adding longitudinal or radial fins to the tube on the local mechanism of melting and solidification is studied. The major phenomena involved in these mechanisms such as natural convection are highlighted and their effects during melting and solidification processes are analysed using the CFD code Star CCM + V12.02. Quantitative analysis including the temporal evolution of the PCM average temperature and the solid volume fraction are analysed and compared for the three configurations. This study exhibits a complex natural convective flow structure in the three storage units due to the inversion of the buoyancy forces in the PCM for the considered temperature range -4 °C to 4 °C. During the solidification process, natural convection intensively develops at the earlier stages of the process and, as the time goes, its effect on the solidification becomes negligible as compared to the one due to conduction. During the melting process, heat is transferred to the PCM first by conduction and later by natural convection. The use of fins significantly increases the solidification and melting rates, especially for the configuration with longitudinal fins for which performance are found to be superior to the two other configurations.

Key-words: PCM, solidification, melting, phase change, CFD, shell and tube, heat exchanger, natural convection, density-temperature inversion.

Nomenclature

C_p	Specific heat capacity	J.kg^{-1}.K^{-1}	T_m	Melting temperature	K
d_1	Distance between the first radial fin and the HTF inlet	m	T_i	Initial temperature	K
d_2	Distance between the second radial fin and the HTF inlet	m	$T_{in,\,c}$	HTF inlet temperature	K
$d_{tubeHTF,in}$	Inner diameter of the HTF tube	m	$t_{fin,long}$	Thickness of longitudinal fins	m
f_L	Liquid volume fraction	-	$t_{fin,rad}$	Thickness of radial fins	m
f_s	Solid volume fraction	-	$\vec{V}$	Velocity vector	m.s^{-1}
$\vec{g}$	Gravitational acceleration vector	m.s^{-2}	$W_{fin,long}$	Width of longitudinal fins	m
H	Material enthalpy	J.kg^{-1}	x,y,z	Cartesian coordinates	m
h	Sensible enthalpy	J.kg^{-1}			
ΔH	Latent heat	J.kg^{-1}			
i,j,k	Unit vectors	-			
l	Specific latent heat	J.kg^{-1}			
$L_{fin,long}$	Length of longitudinal fins	m			
$L_{shell,PCM}$	Length of the PCM shell	m			
$L_{tube,HTF}$	Length of the HTF tube	m			
P	Pressure	Pa			

Greek symbols

ρ	Density	kg.m^{-3}
μ	Dynamic viscosity	Pa.s
λ	Thermal conductivity	W.m^{-1}.K^{-1}
β	Thermal expansion coefficient	K^{-1}

Abbreviations

CFD	Computational fluid dynamics
CFL	Courant–Friedrichs–Lewy condition

$r_{fin,rad}$	Radius of radial fins	m	CLF	Configuration with longitudinal fins
$r_{shell,PCM}$	Radius of the PCM shell	m	CRF	Configuration with radial fins
$r_{tube,HTF,in}$	Inner radius of the HTF tube	m	cop	copper
$r_{tube,HTF,out}$	Outer radius of the HTF tube	m	HTF	Heat transfer fluid
$Re_{d_{tubeHTF,in}}$	Reynolds number based on the inner diameter of the HTF tube	-	LHSU	Latent heat storage unit
t	Time	s	LHTS	Latent heat thermal storage
t_0	Initial time	s	PCM	Phase change material
T	Temperature	K	ref	Reference

1. Introduction

Several researchers have focused their works on thermal energy storage. Thermal energy can be stored under sensible [1-5], latent [6-9], or chemical [10-12] forms. Latent heat thermal energy storage (LHTS) has gained significant attention recently because of its high energy density per unit mass/volume. Indeed, for a given amount of energy, latent heat energy storage system requires a smaller weight and volume of material when compared to a sensible heat energy storage system. Additionally, a latent heat storage system has the ability to store the heat of fusion at a nearly constant temperature that corresponds to the phase change temperature of the material [13]. Hence, different configurations of LHTS units find their wide applications in various engineering fields such as solar based dynamic space power generation, solar thermal application, passive heating of buildings, air conditioning systems, etc. [14]. However, these phase change materials (PCMs) have a low thermal conductivity, which limits the charge and discharge rates during solidification and melting [14]. Various techniques were then adopted in order to enhance the thermal performance of the LHTS units. These techniques are the following: using finned tubes [15-17], employing multiple PCMs in an optimal arrangement [18-19], thermal conductivity enhancement [20-22], and PCMs micro-encapsulation [23-25].

Different LHTS configurations using water as PCM have been studied in the past. Water is used as PCM for low temperature applications because its melting/solidification temperature is about 0 °C. Some researchers have focused their works on rectangular/cubical geometries. Indeed, rectangular module is a basic heat storage unit that is related to various application areas such as solar energy system, geothermal energy, nuclear reactors, etc., because of its simplicity [26]. Cabeza et al. [27] carried out experiments on rectangular latent heat storage unit (LHSU) using water as PCM. The objective was to improve its thermal performance by inserting thermal enhancement materials in the PCM. These enhancement materials were copper pieces, steel pieces, and a graphite matrix impregnated with the PCM, respectively. The main parameters investigated were the temperature evolution at different locations in the heat exchanger during freezing and melting, and the melting/freezing front evolution. According to the authors, the “fin effect” was obtained only by inserting materials with high thermal conductivity such as the case of adding copper or graphite matrix. Furthermore, the most efficient configuration was the one using graphite matrix impregnated with the PCM. Indeed, the system has an additional advantage due to the fact that the graphite matrix forms a consolidated block that allows obtaining uninterrupted heat flux paths, not observable in systems using copper or steel pieces to enhance the heat transfer.

Some other researchers focused their works on cylindrical geometries. Scanlon et al. [28] carried out experimentally and numerically ice melting inside a vertical cylinder. Experimental data of the melting process were obtained using shadowgraphy and particle image velocimetry (PIV) techniques. The numerical model used has taken into account the density inversion effects in the water, which is crucial to simulate the melting phenomenon as water density follows a non-linear path attaining its maximum value at approximately 4 °C. This is one of very few articles dealing with the inversion of the water density around 4 °C. The numerical results show similarity with the experimental results. However, this study focuses only on the flow structure and the evolution of the melting interface. The heat transfer mechanism was not studied.

Some other researchers have focused their works on spherical enclosures. Eames et al. [29] carried out a study in order to characterize the freezing and melting processes of water contained in spherical elements. The main parameters investigated were the ice-wall thickness variation with time during the charging mode, the melt-wall thickness variation with dimensionless time during discharge, energy storage/discharged rate as function of the HTF temperature and the energy storage/charged rate as function of the sphere diameter. The results of this study allow a better comprehension of the phase change process of the water-ice contained in spherical enclosures. A method used to measure the position of the water-ice interface during the solidification process is presented.

Cylindrical shell-and-tube configuration has been experimentally studied using potassium formate/water solution as the HTF and water as the PCM in order to evaluate "dynamical melting concept" [30]. The "dynamic melting concept" consists of recirculating the liquid PCM with a pump in order to increase the overall heat transfer coefficient during the melting process. The results of the study showed significant improvements in efficiency and heat transfer rates, especially when the HTF flow rate was half of the PCM flow rate. It can be concluded that "dynamic melting" is an effective technique for enhancing heat transfer during PCM melting however it requires a supplementary power consumption to actively recirculate the PCM.
The choice of a PCM is mainly related to the temperature level, which depends on the industrial application. Other PCMs than water have been used in such configurations.
Some researchers have focused their works on rectangular/cubical geometries using paraffin as PCM [31-34]. Paraffin is used for medium temperature applications up to 100 °C. Numerical and experimental studies using paraffin as PCM have been also carried out in spherical shells [35] and shell and tubes configurations [36-39]. Some other PCMs (LiF-MgF_2 for example or, $NaNO_3$ etc.) have been used for high temperature applications up to 1000 °C [40-42].

Shell and tube configuration used as a LHSU is a performant configuration, efficient and allows to consider multiple industrial applications for latent heat storage. It is nonetheless crucial to propose simple techniques that can be easily industrialized and that optimize heat transfers during the storage and release phases. Techniques using surface extensions are promising, but it is important to compare different fin configurations in order to find the most effective geometrical configuration. The optimization of these fin configurations must be done using advanced numerical simulation techniques, which will take into account the complex phenomena such as the PCM density variation, the natural convection of the PCM and complex movements at phase change interfaces. The expert use of CFD software tool will allow the optimal design of innovative finned LHSU. The precise numerical analysis will allow to capture the evolution of solidification/melting interfaces during crucial transient phase change periods. The quantitative determination of the performance of several finned LHSU configurations taking into account the effect of density inversion, natural convection in complex confined configurations and conjugated heat transfer will reveal important information for better design and heat transfer intensification of LHSU.

By analysing the literature, very few studies dealt with the inversion of the water density around 4 °C, which is a very important data to be taken into account for low-temperature heat/cold storage in agro-food applications. It has a consequence on the flow structure and thus on the heat transfer mechanism. The few studies found on this subject have focused on the effect of the inversion of the water density around 4 °C on the flow structure without dealing with its effect on the heat transfer mechanism. Furthermore, these studies relate to basic vertical configurations without any heat transfer enhancement by surface extension. In the present study, a three-dimensional numerical analysis of the thermal behaviour of three horizontal shell and tube exchangers, carried out under transient state conditions, is performed for low temperature applications (from -4 °C to 4 °C) with a view to improve the thermal performance of LHTS configurations. One of these storage units, made of a plain tube and a shell is used in this study as the reference against which the other two configurations made respectively of longitudinal and radial finned tube and shell are compared at constant heat transfer surface, compactness and PCM volume. Although some studies can be found in the literature on heat transfer enhancement using surface extension, none of these works analyses, to our knowledge, the influence of the shape of these extensions on the melting-solidification kinetics at constant heat transfer surface, compactness and PCM volume for low-temperature applications in the water density-temperature inversion range. The governing equations were solved using the commercial code Star CCM + V12.02 [43]. The model developed is used to identify and quantitatively evaluate the storage and the heat transfer performance of LHSU used in agro-food industry.

2. Geometry description and boundary conditions

2.1. Geometry description

This work presents a numerical study of a LHSU consisting of a shell-and-tube geometry. The shell space is filled with a phase change material (PCM: water). A heat transfer fluid (HTF: water 75%-glycol 25%) flows by forced convection through the inner tube, and exchanges thermal energy with the PCM. The reference shell and tube unit is presented in Figure 1a and its dimensionless parameters are summarized in Table 1.

HTF		PCM	
$\frac{r_{tube,HTF,out}}{r_{tube,HTF,in}}$	$\frac{L_{tube,HTF}}{r_{tube,HTF,in}}$	$\frac{r_{shell,PCM}}{r_{tube,HTF,in}}$	$\frac{L_{shell,PCM}}{r_{tube,HTF,in}}$
1.17	13.33	6.17	13.33

Table 1 : Dimensionless parameters of the reference heat exchanger

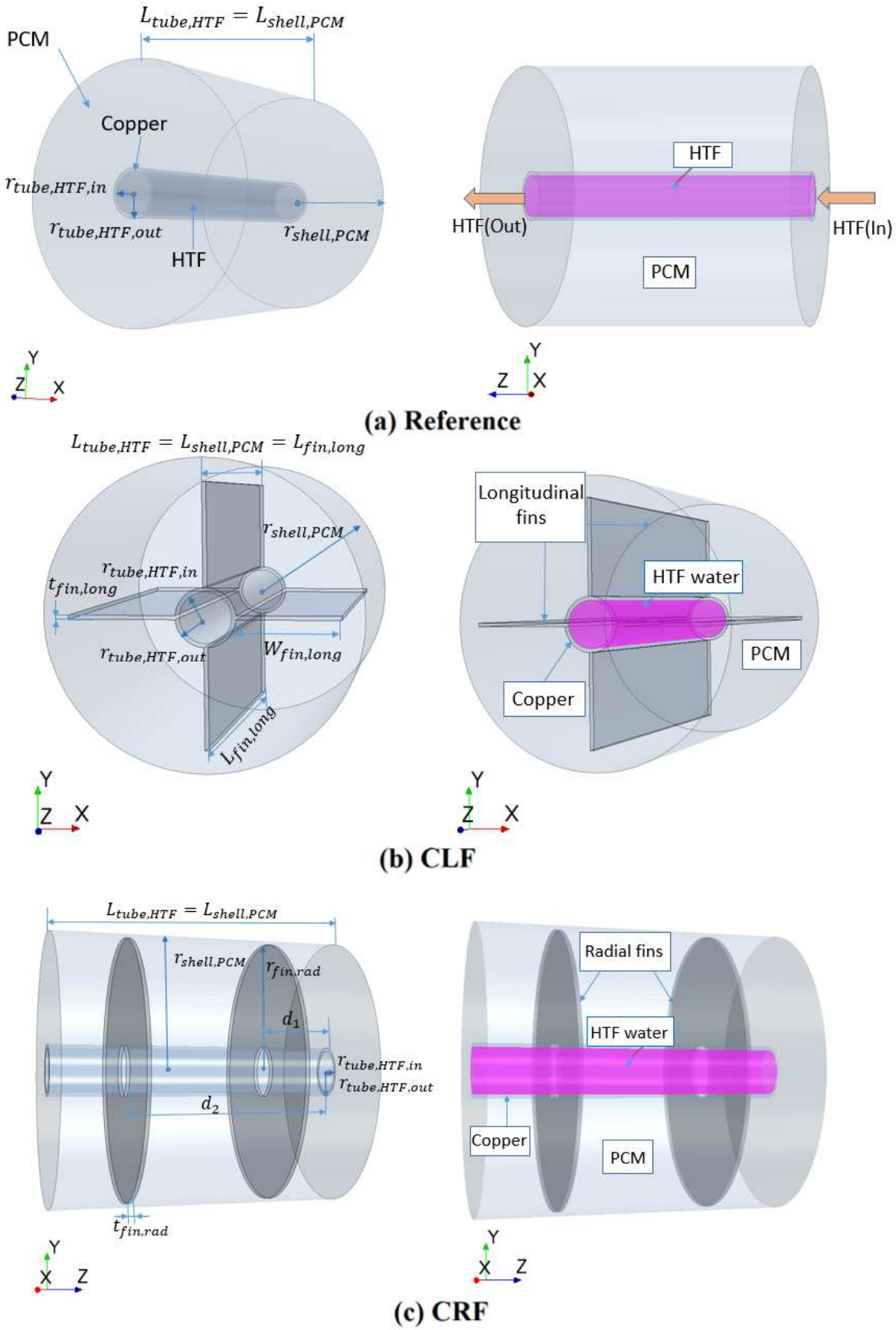

Figure 1 : Illustration of (a) the LHSU reference configuration, (b) the "Configuration with Longitudinal Fins CLF" and (c) the "Configuration with Radial Fins CRF"

A second geometrical configuration of the heat exchanger is derived from the reference geometry by adding longitudinal fins to the HTF tube. This second geometrical configuration will be called "Configuration with Longitudinal Fins" or CLF (Figure 1b).

A third geometrical configuration of the heat exchanger is derived from the reference geometry by adding radial fins to the tube. This third geometrical configuration will be called "Configuration with Radial Fins" or CRF (Figure 1c).

Table 2 summarizes the dimensionless parameters of the fins for the configurations CLF and CRF. It should be noted that the dimensionless parameters of the tube and the PCM are the same as the reference for the two derived configurations so as to keep a constant compactness between the three configurations. In addition, the PCM volume and the total heat transfer surface are also kept constant for CLF and CRF configurations. This will allow to efficiently compare their performance and conclude on the most efficient configuration in terms of heat transfer for equal overall energy storage and compactness.

CLF			**CRF**			
$\frac{L_{fin,long}}{r_{tube,HTF,in}}$	$\frac{W_{fin,long}}{r_{tube,HTF,in}}$	$\frac{t_{fin,long}}{r_{tube,HTF,in}}$	$\frac{r_{fin,rad}}{r_{tube,HTF,in}}$	$\frac{t_{fin,rad}}{r_{tube,HTF,in}}$	$\frac{d_1}{r_{tube,HTF,in}}$	$\frac{d_2}{r_{tube,HTF,in}}$
13.33	4.08	0.17	6	0.17	3.33	10

Table 2 : Dimensionless parameters for the CLF and CRF configurations

Melting and solidification phases were thus simulated in order to characterize the kinetics of heat transfer for the different configurations.

2.2. Physical formulation

In this study, the following assumptions are used: (1) The flow of the heat transfer fluid is modelled through the conservation equations (mass, momentum) in a laminar regime using a water/glycol mixture (75%-25%) as working fluid which is considered incompressible and viscous. (2) The flow of melted/solidified PCM is assumed to be laminar, unsteady and incompressible. (3) Thermophysical properties of HTF [44] and copper [45] are kept constant in the working temperature range. The thermal properties of the solid PCM (ice) [46] and the liquid PCM (water) [47] were taken as a function of temperature. (4) Boussinesq approximation is adopted for the density variation of liquid PCM. (5) The numerical model takes into account the density inversion effects of the water in the vicinity of the melting point. (6) The viscous dissipation and volume change during solid-liquid phase change are neglected.

By considering the above assumption, the conservation equations modelling the flow and heat transfer in the heat exchanger can be written as follows:

- Circulating Heat Transfer Fluid (water/glycol mixture)

$$\nabla.\vec{V} = 0 \tag{1}$$

$$\rho_{HTF}\frac{\partial \vec{V}}{\partial t} + \rho_{HTF}(\vec{V}.\nabla)\vec{V} = -\nabla P + \mu_{HTF}\nabla^2\vec{V} \tag{2}$$

$$\frac{\partial T}{\partial t} + \vec{V}.\nabla T = \frac{\lambda_{HTF}}{\rho_{HTF}C_{p,HTF}}\nabla^2 T \tag{3}$$

- HTF tube (copper)

$$\frac{\partial T}{\partial t} = \frac{\lambda_{cop}}{\rho_{cop}C_{p,cop}}\nabla^2 T \tag{4}$$

- PCM: Distilled water: Pure substance

$$\nabla.\vec{V} = 0 \tag{5}$$

$$\rho_{PCM}\frac{\partial \vec{V}}{\partial t} + \rho_{PCM}(\vec{V}.\nabla)\vec{V} = -\nabla P + \mu_{PCM}\nabla^2\vec{V} + \rho_{PCM}\vec{g}\beta(T_{ref} - T) \tag{6}$$

$$\frac{\partial H}{\partial t} + \nabla(\vec{V}h) = \nabla\left(\frac{\lambda_{PCM}}{\rho_{PCM}C_{p,PCM}}\nabla h\right) \tag{7}$$

The enthalpy of the material is computed as the sum of the sensible enthalpy, h, and the latent heat ΔH.

$$H = h + \Delta H \tag{8}$$

$$h = h_{ref} + \int_{T_{ref}}^{T} C_{p,PCM}\, dT \tag{9}$$

The latent heat content can be written in terms of the specific latent heat of the material, *l,* and the liquid volume fraction, $f_{L,}$ as follows:

$$\Delta H = f_L . l \tag{10}$$

In the present study, distilled water is used as PCM, which is a pure substance. The melting and solidification processes take place at a constant temperature. So, depending on the temperature, there is either liquid or solid in the computational domain and, therefore, the function $f_L(T)$ is defined as follows:

$$f_L(T) = \begin{cases} 1 \text{ si } T > T_m \\ 0 \text{ si } T < T_m \end{cases} \tag{11}$$

The "Melting and Solidification model" is used in STAR CCM+ [43]. This model simulates only the effect of phase change on the energy equation as shown in the equation (7); it does not modify the momentum equations.

For impure substances, the melting and solidification process is not instantaneous but takes place over a period of time. During this time, the phase mixture can influence the flow field. Depending on the value of the solid fraction (specifying to which extent the liquid has solidified), two models are available in STAR CCM+ [43]:

- The slurry viscosity Model that uses Metzner method is implemented to increase the viscosity for low values of solid fraction up to the critical solid fraction (approximately 0.3) [43] when the mixture is considered as a slurry, where solid grains are suspended in the melt, nearly without interacting with each other.
- The Mushy Zone Permeability Model is implemented for solid fractions above the specified critical solid fraction (approximately 0.3) [43]. The mushy zone is a partially solidified stationary region permeated with dendrites. For these values of solid fraction, the flow resistance in a mushy zone can be modeled similar to an isotropic porous medium, using the Carman-Kozeny Mushy Zone Permeability method [43].

For the present simulation, partial solidification is not present as the PCM considered is a pure substance. However, in the presence of pressure gradients, or body forces such as gravity, a creeping flow develops independently of the magnitude of slurry viscosity or mushy zone permeability. To prevent creeping flows, an additional flow stop functionality is used [43]. The Melting-Solidification Flow Stop model is activated above a specified flow stop solid fraction f_s of 0.999 [43]. Finally, in the present study, the buoyancy forces appearing in equation (6) that create natural convection in the PCM were modeled as a momentum source term using additional user's field function.

2.3. Initial and boundary conditions

2.3.1. Solidification process

The following initial and boundary conditions are considered during the solidification process.

- Initial conditions

At the initial time t_0=0s, the three configurations are supposed to be at an initial uniform temperature T_i(x, y, z, 0) = 4 °C.

- Boundary conditions

At the inlet of the cooling heat transfer fluid, Poiseuille velocity profile is imposed. This velocity corresponds to a Reynolds number $Re_{d_{tube,HTF,in}} = 1000$ based on the inner diameter of the HTF tube. A constant inlet temperature $T_{in,\,c}$ = - 4 °C is imposed at the inlet of the cooling heat transfer fluid while a pressure outlet boundary condition is considered at the outlet. At all fluid-solid and solid-solid interfaces, conjugate heat transfer is considered. All the external boundaries of the PCM volume are considered to be adiabatic.

2.3.2. Melting process

The following initial and boundary conditions are considered during the melting process.

- Initial conditions

At the initial time, the three configurations are supposed to be at an initial uniform temperature $T_i(x, y, z, 0)$ = -4 °C.

- Boundary conditions

At the inlet of the heating heat transfer fluid, Poiseuille velocity profile is imposed. This velocity corresponds to a Reynolds number $Re_{d_{tube,HTF,in}} = 1000$ based on the inner diameter of the HTF tube. A constant inlet temperature $T_{in,c} = 4$ °C is imposed at the inlet of the heating heat transfer fluid while a pressure outlet boundary condition is considered at the outlet. At all fluid-solid and solid-solid interfaces, conjugate heat transfer is considered. All the external boundaries of the PCM volume are considered to be adiabatic.

3. Numerical procedure

3.1. Numerical scheme and solvers

The commercial code STAR-CCM + V12.02 was used to solve the above conservation equations based on a finite volume discretization method. The conservation equations were solved sequentially using the AMG algebraic solver and the SIMPLE algorithm for pressure-velocity coupling. A second-order discretization was chosen for the convective terms of the momentum and energy equations. A temporal discretization of second order was chosen.

3.2. The code validation

In order to validate the ability of our finite volume CFD code to model phase change, a preliminary numerical simulation of the melting process of tin in a square cavity heated from the side was performed and compared with the well-known phase change benchmark of Hannoun et al. [48] taken as the reference case for comparison. A study of the grid and time step sensitivity was carried out. This study led to the use of a 500 x 500 grid and a time step of 0.01 s, which allows to precisely capture the evolution of the melting front and the flow structure. The problem begins with fully solid tin at its melting temperature in the cavity. Heating the left boundary to a temperature above the melting point initiates melting.
Figure 2 shows a comparison of the liquid fraction at different times between the two studies. It can be observed that the comparison results exhibit a satisfactory correspondence with a maximum discrepancy of 0.86 % between both studies.

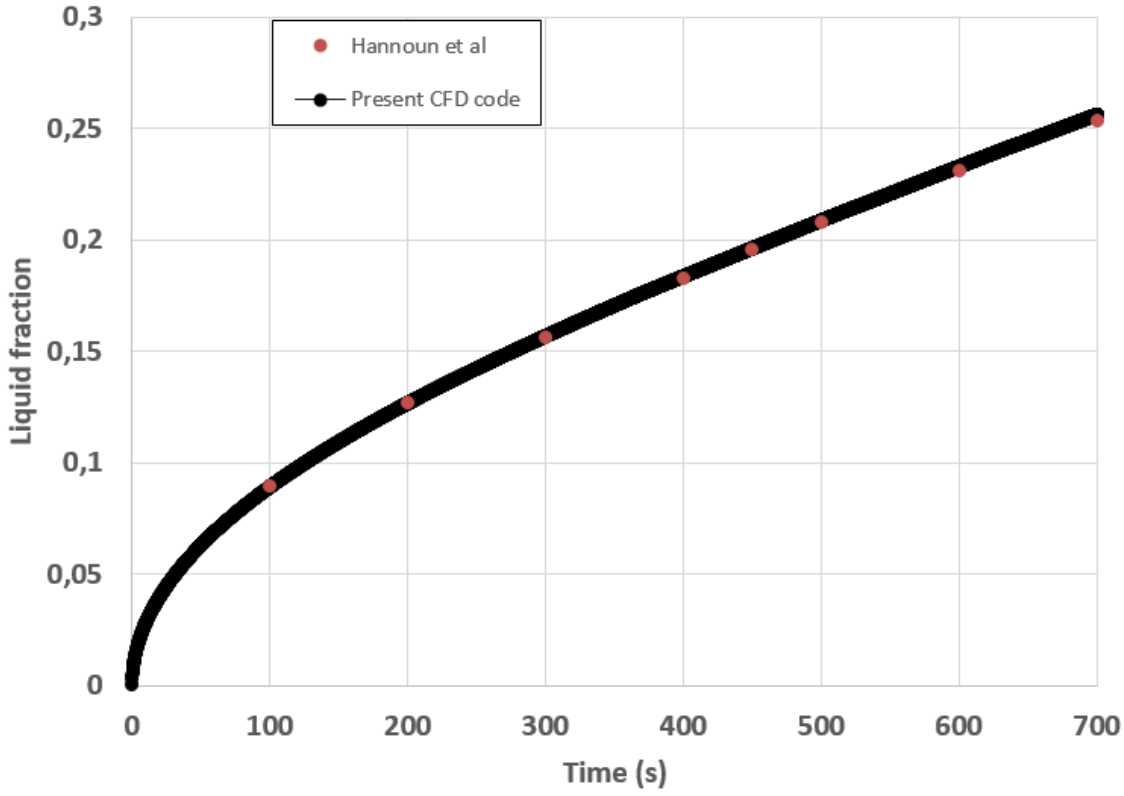

Figure 2 : Liquid fraction vs. time

In order to better qualify our numerical procedure, Figure 3 shows a qualitative comparison of the recirculation cells at two different times between the two studies. The results clearly show that the finite volume CFD code used allows capturing the vortices which develop locally over time, therefore confirming the ability of the CFD code to accurately model phase change.

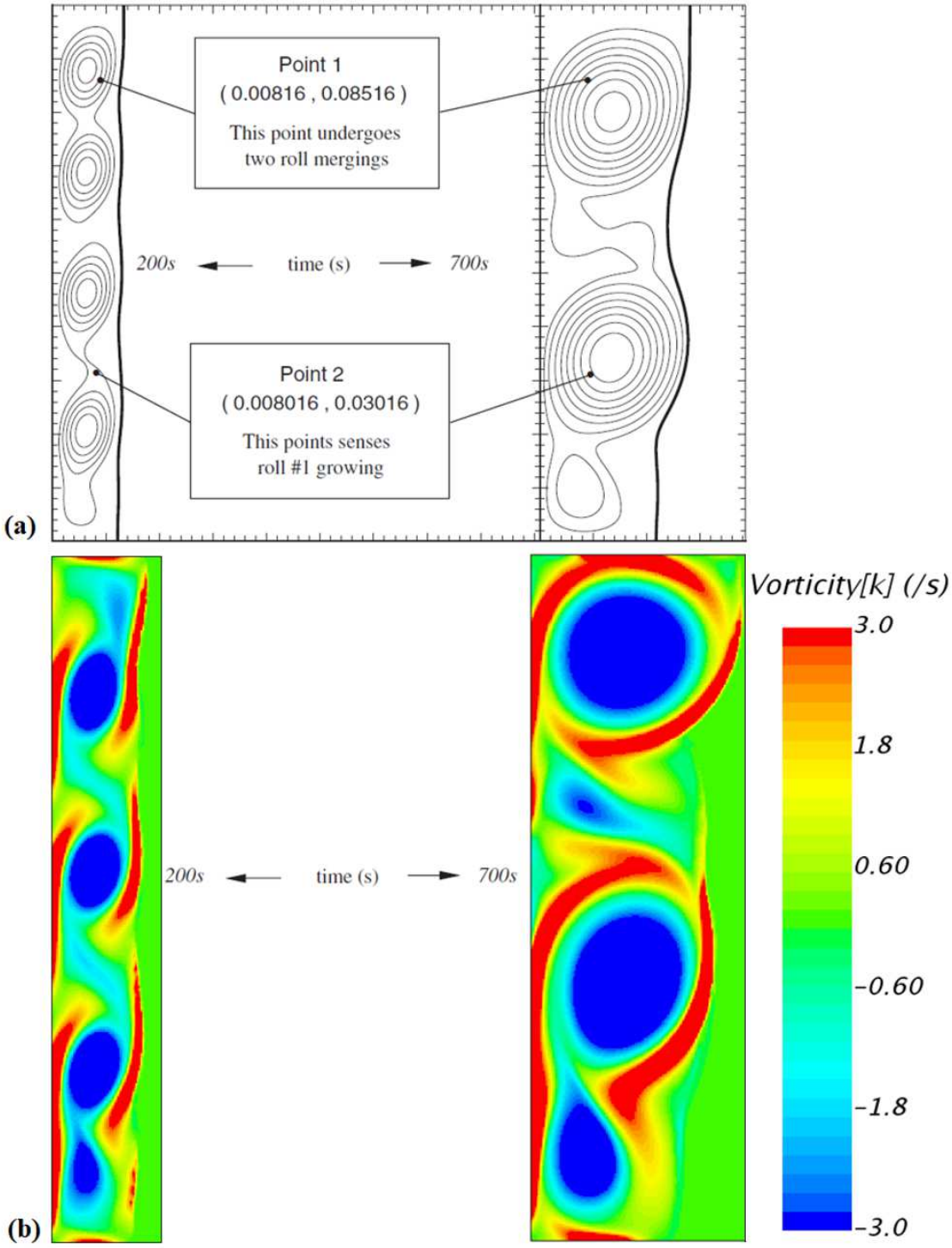

Figure 3 : Recirculation cells at different times (a) Benchmark results (Hannoun et al. [48]) (b) Present code

3.3. Grid and time step sensitivity

A grid and time step sensitivity study was carried out during solidification process for the CLF configuration by the fact that it is, phenomenologically, the most complex configuration. The grid sensitivity was performed for a Reynolds number $\mathrm{Re}_{d_{tube,HTF,in}} = 1000$ based on the inner diameter of the HTF tube. The appropriate grid was chosen based on the solid volume fraction of the PCM.

By performing a gradual refinement of the mesh, a set of three grid systems having respectively 0.5; 1.1 and 1.6 Million of cells were generated in the computational domain. The difference in the solid volume fraction

between the grid system with 1.1 Million and the one with 1.6 Million of cells did not exceed 1 %. Taking into account the available computing resources, it was decided to use the configuration having 1.1 Million cells throughout the study.

Figure 4 illustrates the retained grid distribution in two median planes for the reference geometry: a vertical and a horizontal median planes. For copper region, the "thin layer mesher" [43] was used. This type of mesh is typically used in order to generate a prismatic type volume mesh for thin volumes within parts or regions [43] of the computational domain. For the PCM and the HTF, the trimmed cell mesher [43], which generates hexahedral cells, was used. The trimmed cell mesher provides a robust and efficient method of producing a high-quality grid for both simple and complex mesh generation problems.

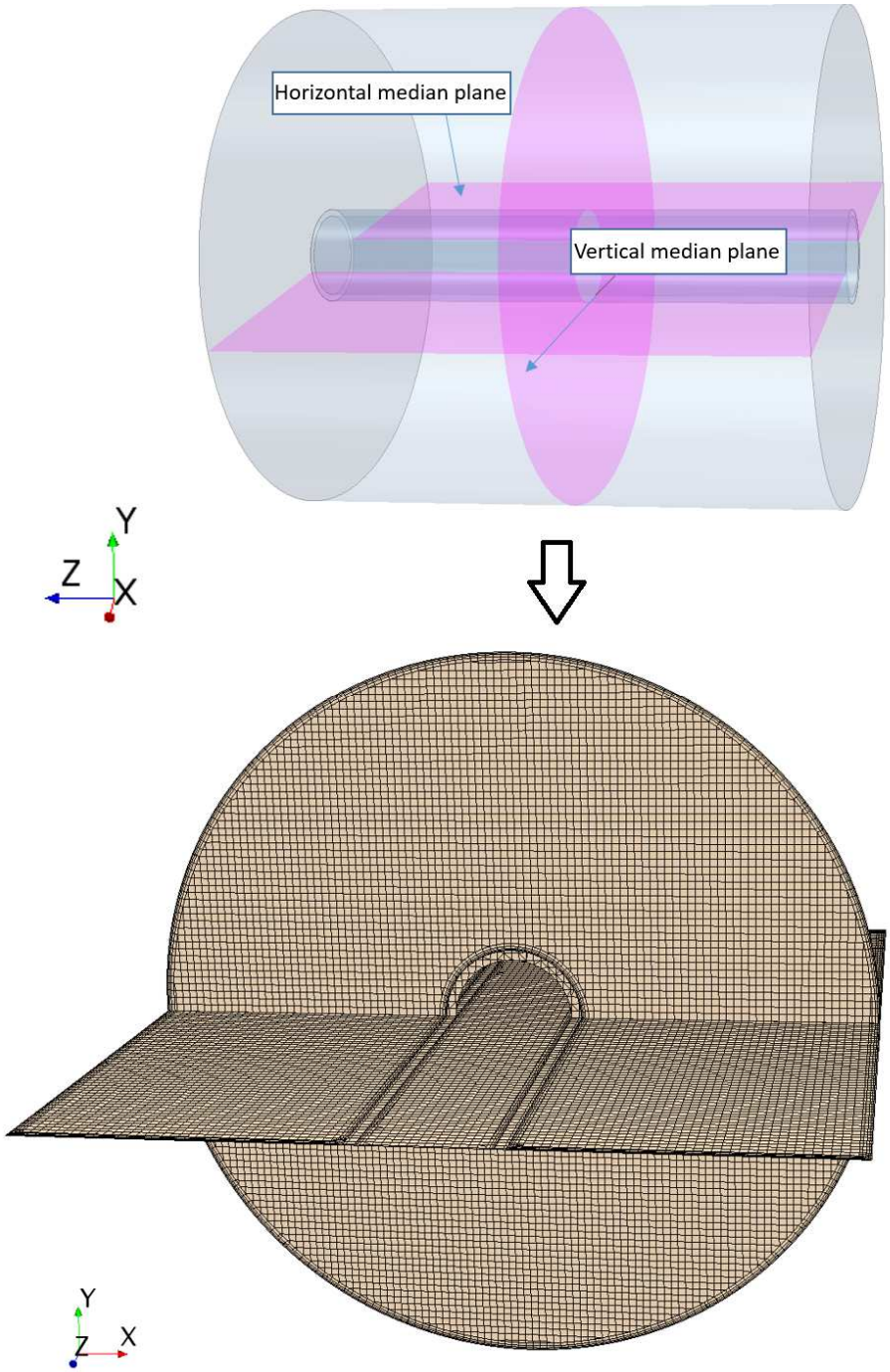

Figure 4 : Grid distribution in two median planes for the reference geometry

Moreover, since the precision of the results is intimately related to the time step chosen for unsteady calculations, a time step sensitivity study was carried out using the optimal above grid and a succession of three time steps of 0.4 s; 0.2 s and 0.1 s. This study led to the use of a time step of 0.2 s corresponding to a maximum CFL of 0.02 in the PCM, and a maximum inner iterations of 100 for each time step owing the fact that melting and solidification processes require more inner iterations compared to unsteady single phase simulations [43].

4. Results

In this section, quantitative and qualitative results will be presented. Since this study is intended to analyse the latent thermal storage, we will focus, in the following, on the transient operation of the three heat exchangers due to the fact that the unsteady state operation is of capital importance for latent heat storage.

4.1. Local mechanisms of conducto-convective heat exchanges

4.1.1. Solidification process

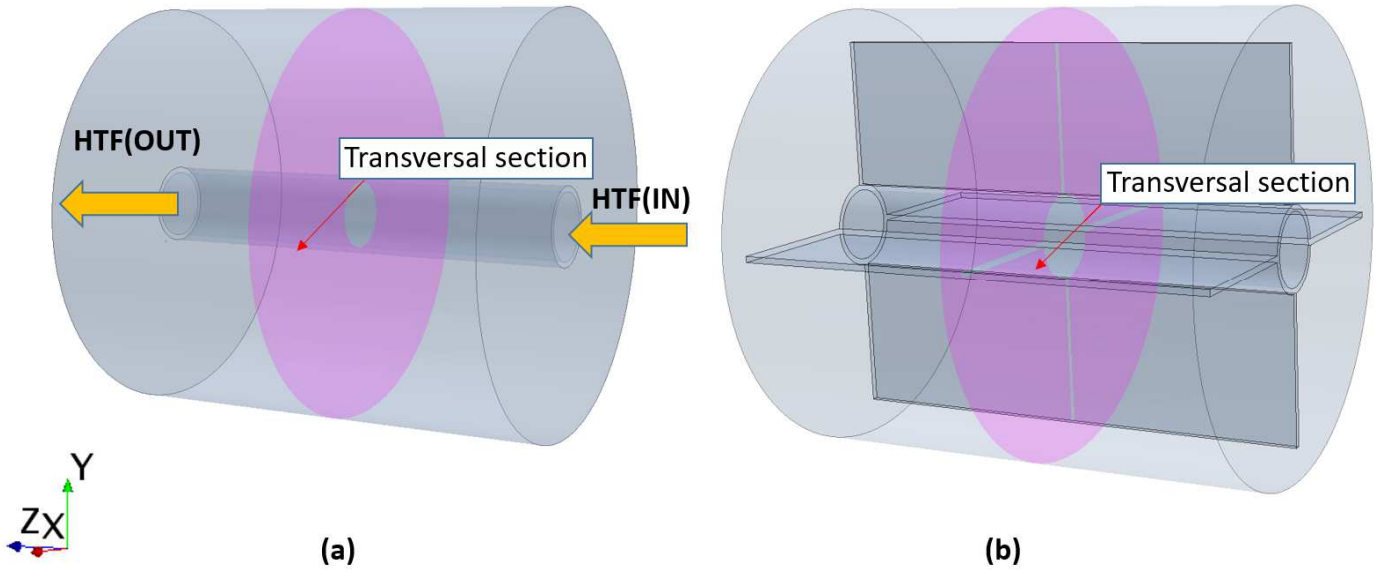

Figure 5 : Illustration of the transversal middle cross-section for the (a) reference and (b) CLF configurations

This part of the analysis will focus on the presentation of the local heat transfer mechanism that occurs in these shell and tube LHTS units. The solid state PCM (ice) growth, temperature contours and streamlines are presented in the transversal middle cross-section of the unit (presented in Figure 5) at different times. The velocity contours are also presented since they provide information on the intensity of natural convection in the liquid PCM.

The first part of this section is devoted to compare the reference with the CLF configuration during the solidification process.

Figures 6a and 6b show the ice growth over time in the transversal middle cross-section (presented in Figure 5) during solidification for the reference and the CLF configurations respectively. Blue and red regions represent respectively the liquid and solid phases of the PCM. Also, it is important to recall that the Reynolds number of the HTF is $\mathrm{Re}_{d_{tube,HTF,in}} = 1000$ and density-temperature inversion of water is taken into consideration for natural convection. As the HTF does not undergo phase change, it is not presented in Figures 6a and 6b. We can notice that the ice formation is not axisymmetric for the reference configuration, but almost symmetric for the CLF configuration. For both configurations, conduction is therefore not the only heat transfer mechanism, especially for the reference configuration. The asymmetry of the ice thickness with respect to y-axis is mainly due to the development of natural convection. It can also be seen in Figures 6a and 6b that the ice formation is more significant in the upper part compared to the lower part particularly for the reference configuration. This is the consequence of the density inversion of the PCM (water) at lower temperature range ($0 < T < 4$ °C), where the increase of the liquid PCM density with respect to temperature leads to negative values of the thermal expansion coefficient, otherwise to ascending flow in the vicinity of the cooling HTF tube. As expected, a rapid growth of ice is observed in CLF configuration compared to the reference LHTS unit indicating a heat transfer enhancement due to the fins in the CLF configuration.

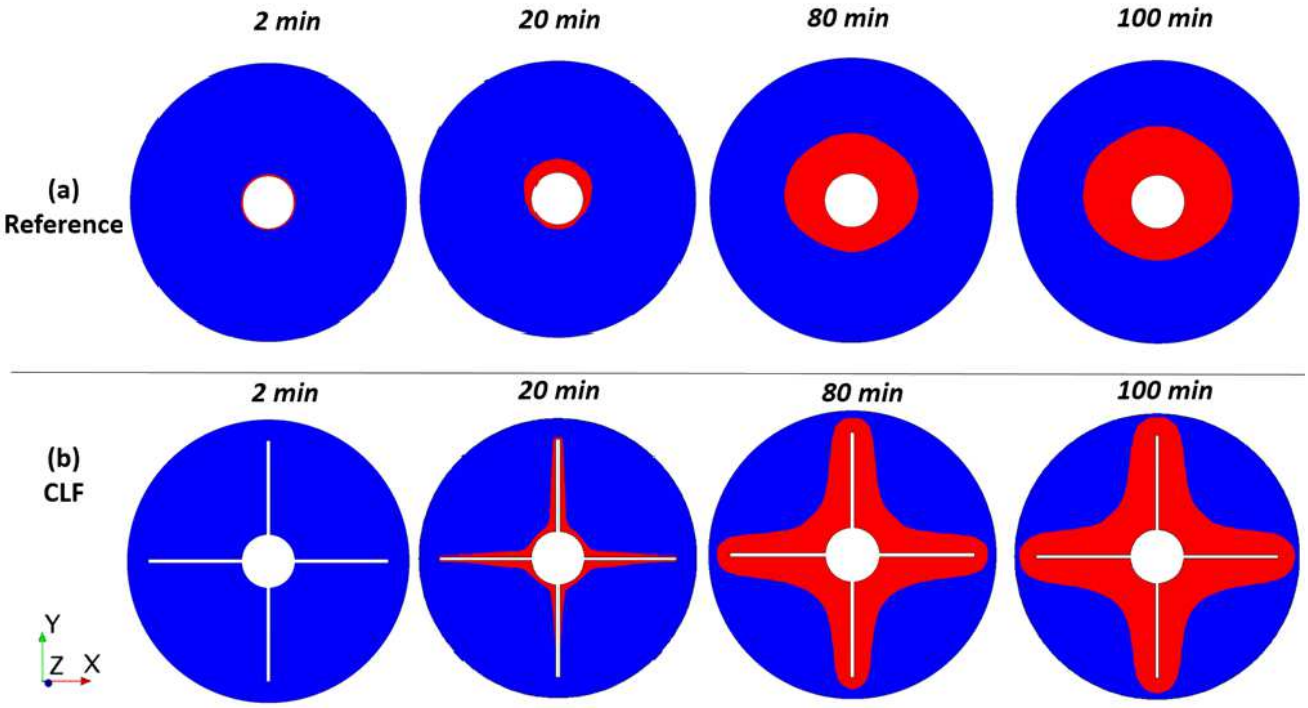

Figure 6 : Illustration of the ice growth in the transversal middle cross-section during solidification for the (a) reference and (b) CLF configurations

Figures 7a and 7b show the velocity contours over time in the transversal middle cross-section (presented in Figure 5) during solidification respectively for the reference and the CLF configurations. An asymmetry of the velocity field is visible with high values of velocity magnitude in the top region of the PCM compared to the bottom region indicating vigorous ascending flow at the earlier stages of the solidification process. This situation is more visible in the reference configuration compared to the CLF configuration as the presence of a fin in the bottom region of the CLF configuration enhances the natural convection compared to the bottom region of the PCM reference configuration. This is the reason of less asymmetry in the ice thickness for the CLF configuration compared to the reference configuration (see Figure 6b). Hence, the presence of longitudinal fins reduces this asymmetry effect and thus would allow to intensify the heat exchange and to reduce the solidification time.

For both configurations, the effect of the natural convection is more significant at the earlier stages of the solidification process. Natural convection exists only in the very beginning of the solidification process, and as the time goes, its intensity progressively vanishes. Such behaviours have also been reported in some other studies [49-50].

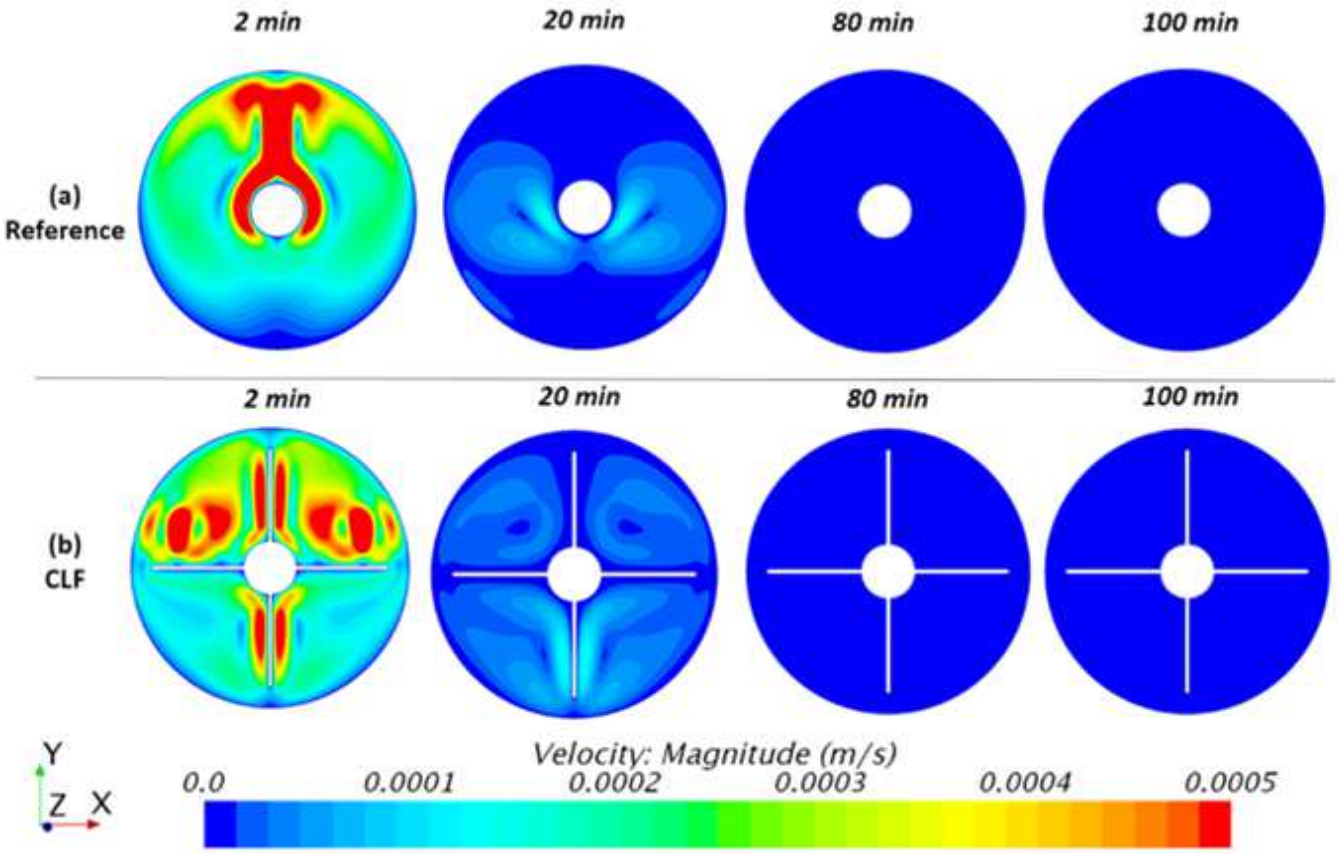

Figure 7 : Illustration of the velocity contours over time in the transverse middle cross-section during solidification for the (a) reference and (b) CLF configurations

Figures 8a and 8b show the temperature distribution (and streamlines in black colour) over time in the transversal middle cross-section (presented in Figure 5) during solidification respectively for the reference and the CLF configurations. The temperature gradients are higher at the beginning of the solidification process when natural convection is intense. The highest temperature levels are found in the lower part of the PCM because of the density-temperature inversion of the PCM in the temperature range 0 to 4 °C that leads to negative values of the thermal expansion coefficient as discussed before.

For the reference configuration, two large symmetrical vortices are present at the beginning of the solidification process. The centres of these vortices are located in the top region of the PCM indicating an upward movement of the fluid at the beginning of the solidification process due to density-temperature inversion of the PCM in the range 0-4 °C. Over time, each large vortex splits into two vortices, thus forming four vortices. Then, the vortices divide further to form six vortices. The two upper vortices are smaller due to the fact that the thicker solidified layer at the top region of the PCM decreases the free fluid path in the upper region compared to the lower region.

For the CLF configuration, small symmetrical vortices with respect to vertical fins are present. Asymmetry is present with respect to horizontal fins. The vortex movement is more present in the upper part of the plane, as for the reference configuration, proving the upward movement of the fluid at the start of convection. Over time, as the temperature gradients decrease, natural convection decays leading to four vortex structures each one delimited by adjacent fins. The asymmetry between the upper and lower vortices is less marked over time as observed for the reference configuration due to the fact that the difference between the thicknesses of the solidified layers is less pronounced than for the reference case.

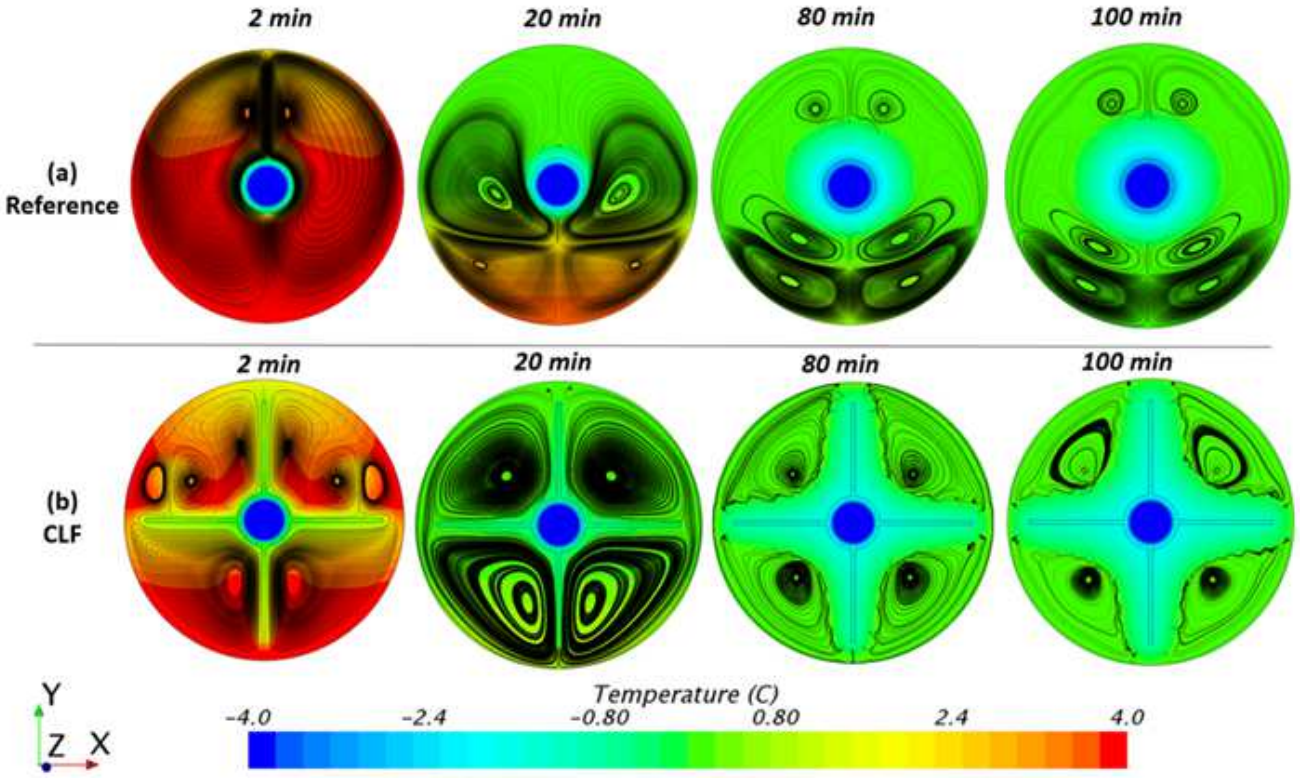

Figure 8 : Temperature distribution and streamlines evolution in the transverse middle cross-sectional plane during solidification for the (a) reference and (b) CLF configurations

The second part of this section is devoted to compare the reference configuration with the CRF configuration during the solidification process.

Figures 10a and 10b show the ice growth over time in the longitudinal median plane (presented in Figure 9) during solidification respectively for the reference and the CRF configurations. The blue colour in Figures 10a and 10b represents the liquid PCM and the red colour represents the solid PCM. The heat transfer fluid is not presented in Figures 10a and 10b. We can notice that the ice formation is not axisymmetric for the reference configuration, but almost symmetric for the CRF configuration. Hence, the presence of radial fins reduces this asymmetry effect and thus would allow to intensify the heat exchange and reduce the solidification time. It can also be seen that the ice formation is more significant in the upper part compared to the lower part especially for the reference configuration. This is the consequence of the density inversion of the PCM (water) at lower temperature range ($0 < T < 4$ °C), where the increase of the liquid PCM density with respect to temperature leads to negative values of the thermal expansion coefficient, otherwise to ascending flow in the vicinity of the cooling HTF tube. One can also notice that the solidified layer is thicker at the inlet of the HTF compared to the outlet as the result of the heat transfer decrease along the HTF tube wall.

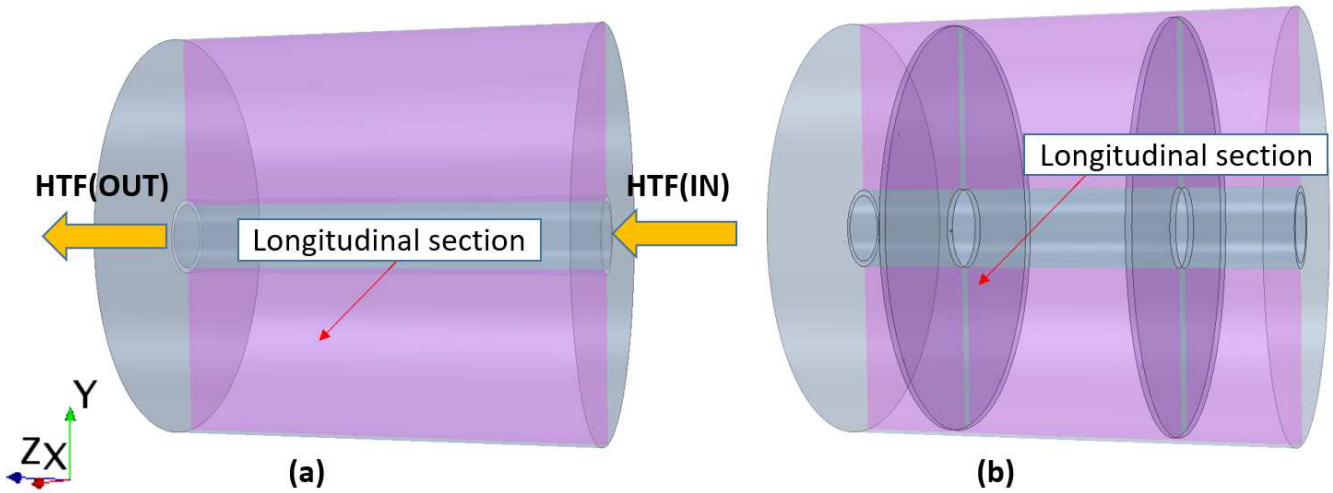

Figure 9 : Illustration of the longitudinal median plane for the (a) reference and (b) CRF configurations

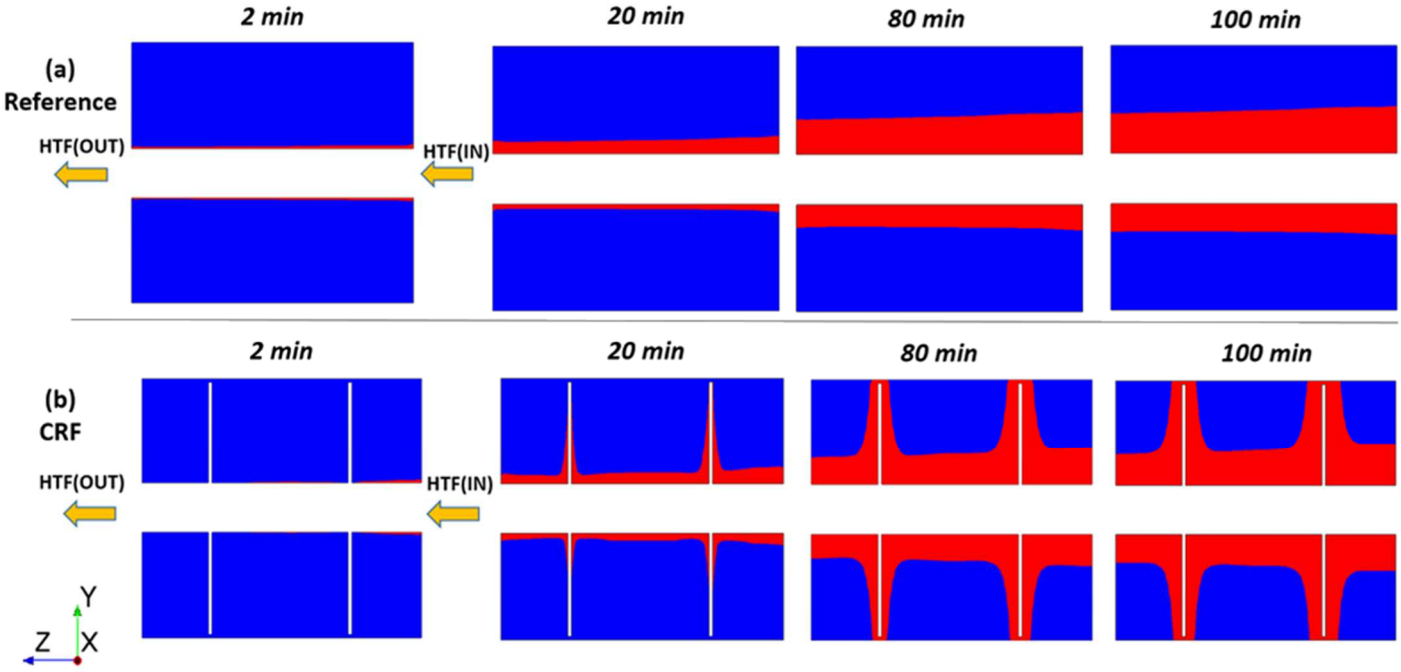

Figure 10 : Illustration of the ice growth in the longitudinal median plane during solidification for the (a) reference and (b) CRF configurations

Figures 11a and 11b show the velocity contours over time in the longitudinal median plane presented in Figure 9 during solidification for the reference and the CRF configurations respectively. For the two configurations, an asymmetry of the velocity field is visible at the beginning of the process with high values of velocity magnitude in the top region of the PCM indicating vigorous ascending flow compared to the bottom region. The effect of the natural convection is significant at earlier stages of the solidification process. Natural convection exists only in the beginning and as the time goes, the effect of natural convection progressively vanishes. It is interesting also to note that the presence of the fins increases the time during which the natural convection is not negligible, which will improve the efficiency of thermal storage.

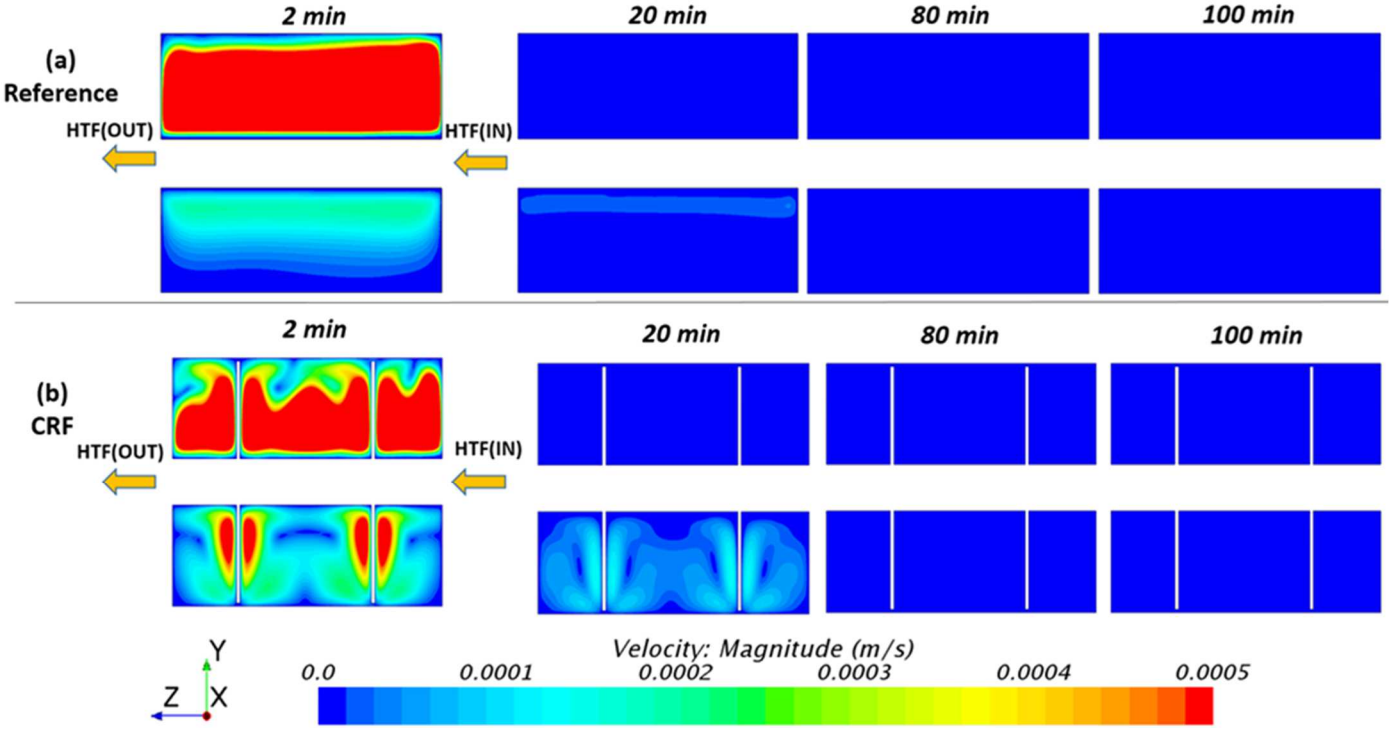

Figure 11 : Illustration of the velocity contours over time in the longitudinal median plane during solidification for the (a) reference and (b) CRF configurations

4.1.2. Melting process

The first part of this section is devoted to compare the reference with the CLF configuration during the melting process.

Figures 12a and 12b show the ice melting over time in the transversal middle cross-section plane (presented in Figure 5) for the reference and the CLF configurations respectively. The blue and red colours represent respectively the liquid and the solid phases of the PCM. Also, it is important to recall that the Reynolds number of the HTF is $\mathrm{Re}_{d_{tube,HTF,in}} = 1000$ and density-temperature inversion of water is taken into consideration for natural convection. As the HTF does not undergo phase change, it is not presented in Figures 12a and 12b. We can notice that the ice melting is axisymmetric only during the first twenty minutes for the two configurations due to the fact that the volume of the melted PCM is thin and natural convection is negligible compared to the conduction. Over time, it can be noticed that the ice melting begins to be no longer symmetrical for the two configurations. Conduction is therefore not the only heat transfer mechanism. Natural convection is involved in the melting process. The asymmetry of the ice melting with respect to y-axis is mainly due to the progressive development of natural convection. It can also be seen in Figures 12a and 12b that the ice melting is more significant in the lower part compared to the upper part. This is the consequence of the density inversion of the PCM (water) at lower temperature range ($0 < T < 4$ °C), where the increase of the liquid PCM density with respect to temperature leads to negative values of the thermal expansion coefficient, otherwise to descending flow in the vicinity of the heating HTF tube. As expected, a rapid ice melting is observed in the CLF configuration compared to the reference LHTS unit, indicating a heat transfer enhancement by fins in the CLF configuration.

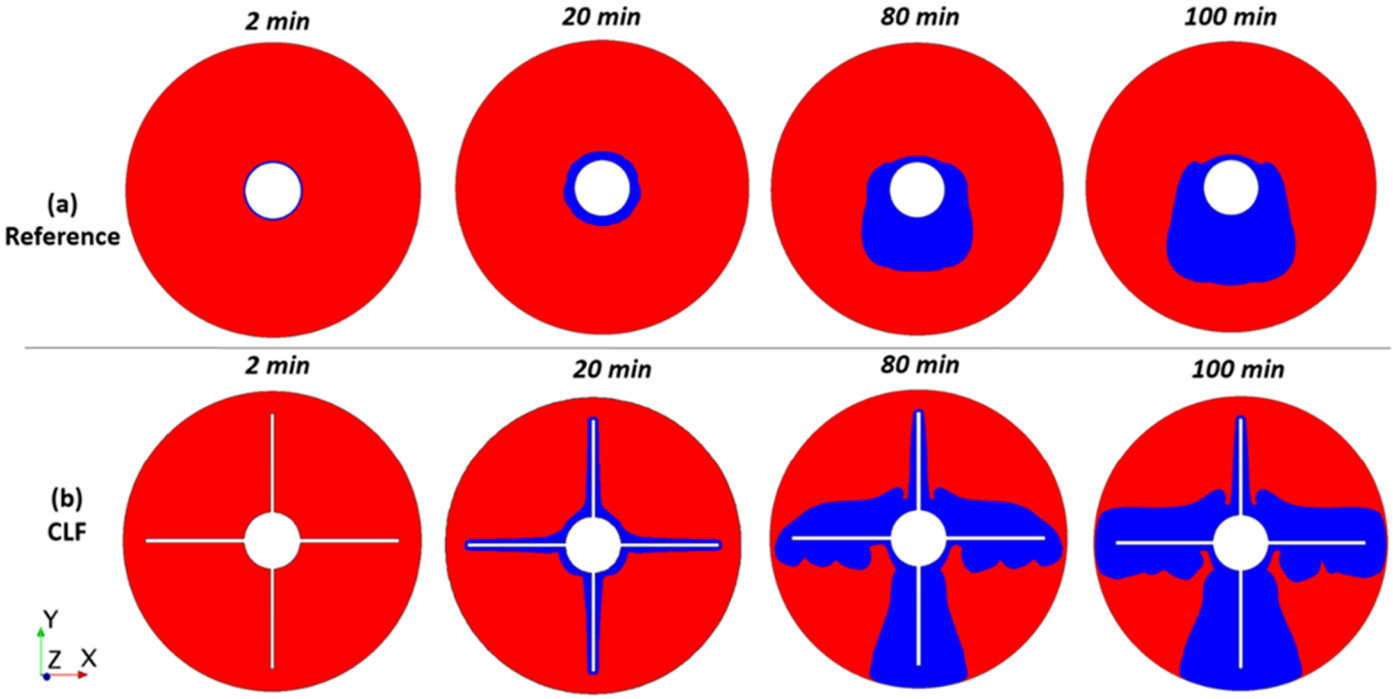

Figure 12 : Illustration of the ice melting in the transversal middle cross-section for the (a) reference and (b) CLF configurations

Figures 13a and 13b show the velocity contours over time in the transversal middle cross-section plane (presented in Figure 5) during melting respectively for the reference and the CLF configurations. For the two configurations, the effect of the natural convection is negligible at earlier stages of the melting process as the first liquid PCM layers are mainly dominated by viscous forces that make conduction to be the main heat transfer mechanism. Over time, the effect of natural convection becomes more noticeable as a result of the increase of buoyancy forces with the increase of the thickness of the melted PCM. In contrast to the solidification process where natural convection is intense at the early stages of the solidification, during the melting process, natural convection becomes increasingly intense with the increase of the volume of melted PCM. Such behaviours have also been reported in some other studies [50-51].

An asymmetry of the velocity field is visible with high values of velocity magnitude in the bottom region of the PCM compared to the top region indicating vigorous descending flow. This situation is more visible in

the reference configuration compared to the CLF configuration as the presence of a fin in the top region of the CLF configuration enhances the natural convection compared to the top region of the PCM reference configuration. This is the reason of less asymmetry of ice melting in the CLF configuration compared to the reference configuration. Hence, the presence of longitudinal fins reduces the asymmetry effect and thus would allow to intensify the heat exchange and reduce the melting time.

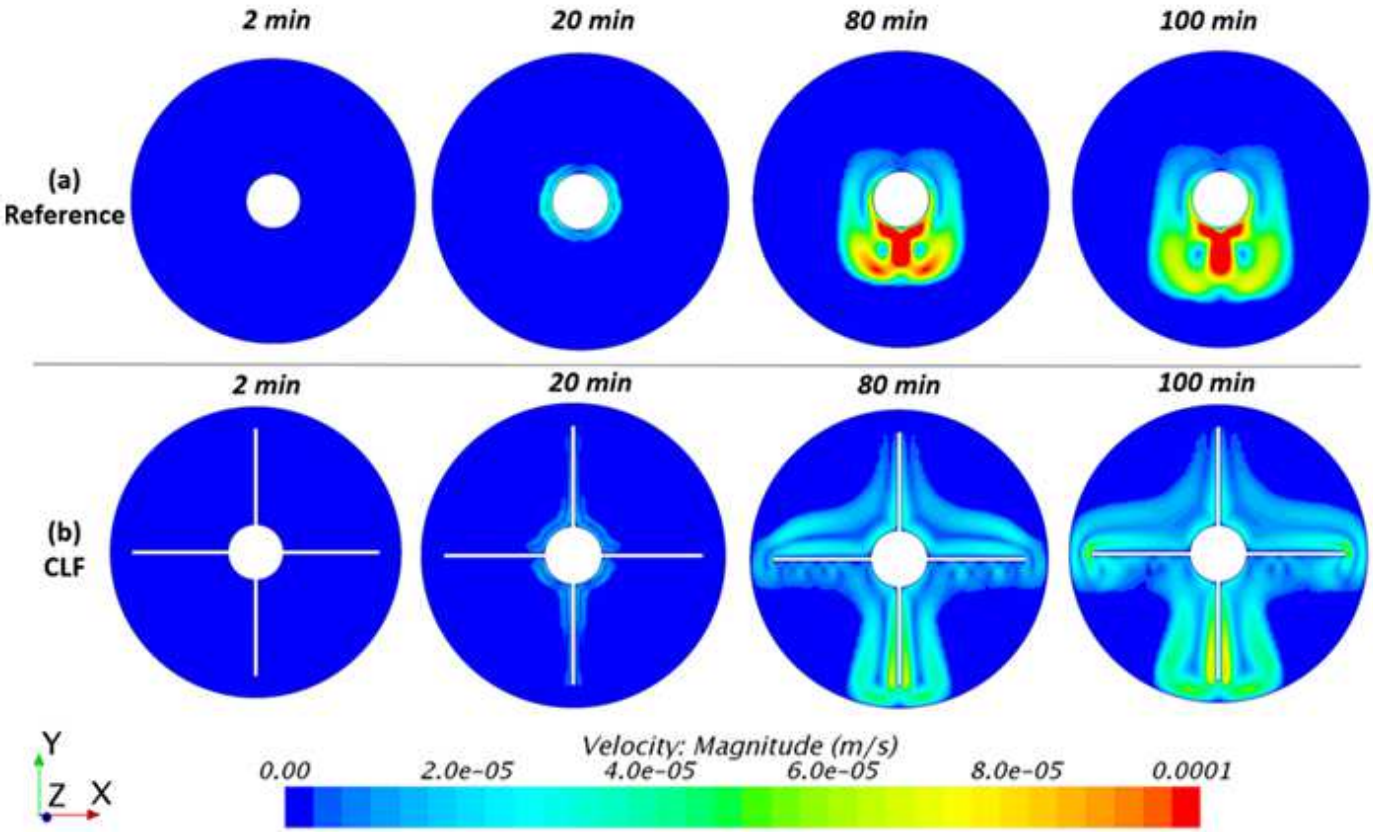

Figure 13 : Illustration of the velocity contours over time in the transversal middle cross-section during melting for the (a) reference and (b) CLF configurations

Figures 14a and 14b show the temperature distribution (and streamlines in black colour) over time in the transversal middle cross-section plane presented in Figure 5 during melting respectively for the reference and the CLF configurations. The temperature gradients are higher at the beginning of the melting process. The temperature field is symmetrical and takes the form of the heat exchange surface.

For the reference configuration, and over time, two symmetrical vortices begin to form with increasing water volume of melted PCM. The centres of these vortices are located in the lower part in the fluid volume resulting from the melting process. The significant difference in the thickness of the melted PCM between regions under and above the HTF tube is the result of a downward motion of the melted PCM in the vicinity of the tube and an upward motion in the vicinity of the melting front, as a consequence of the negative values of the thermal expansion coefficient of water for temperature below 4 °C, that generate the two vortices. These vortices continue to increase over time leading to more significant ice melting in the lower part compared to the upper part.

For the CLF configuration, and as for the reference configuration, the temperature gradients are higher at the beginning of the melting process. The temperature field is symmetrical and takes the form of the heat exchange surface. Over time, vortices start to form. The shapes and grip of the vortices on the volume are not at all similar between the top and the bottom. The vortex movement is stronger in the lower part of the plane. It is interesting also to note that there is less surface unaffected by vortices at the top of the CLF configuration compared to the reference configuration.

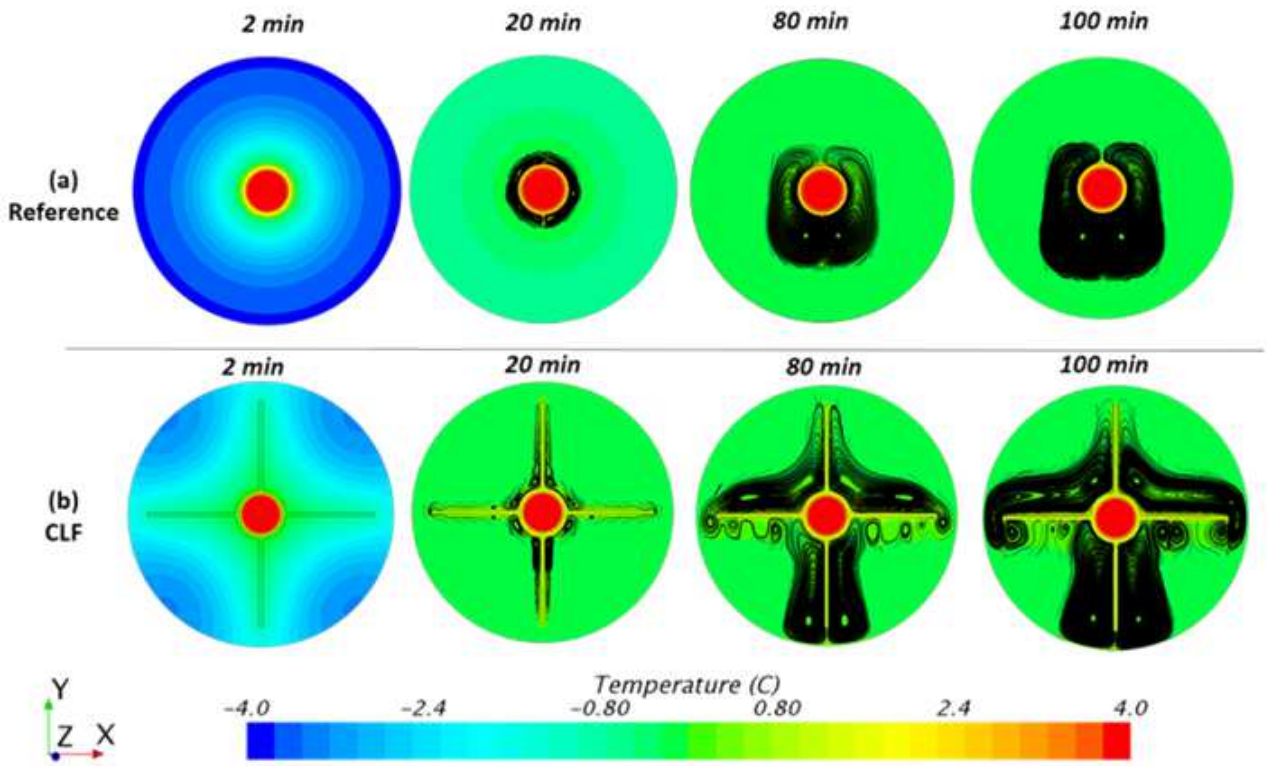

Figure 14 : Temperature distribution (and streamlines) over time in the transversal middle cross-section during melting for the (a) reference and (b) CLF configurations

The second part of this section is devoted to compare the reference with the CRF configuration during the melting process.

Figures 15a and 15b show the ice melting over time in the longitudinal median plane presented in Figure 9 respectively for the reference and the CRF configurations. The blue and red colours respectively represent the liquid and solid phases of the PCM. The heat transfer fluid is not presented in Figures 15a and 15b. One can notice that, over time, the ice melting is no longer symmetrical for the two configurations. Therefore, natural convection is involved in the melting process. The ice melting is more significant in the lower part compared to the upper part. This is the consequence of the density inversion of the PCM (water) at lower temperature range ($0 < T < 4$ °C), where the increase of the liquid PCM density with respect to temperature leads to negative values of the thermal expansion coefficient, otherwise to descending flow in the vicinity of the heating HTF tube as discussed above. One can also notice that the melted layer is thicker at the inlet of the HTF compared to the outlet as the result of the heat transfer decrease along the HTF tube wall.

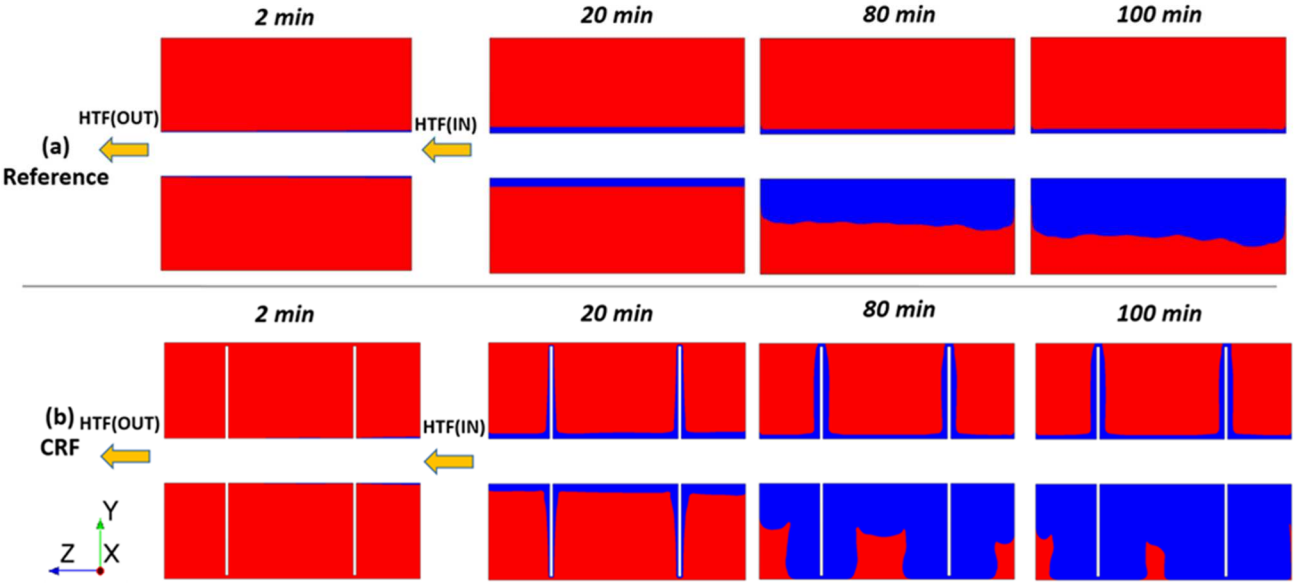

Figure 15 : Illustration of the ice melting in the longitudinal median plane during melting for the (a) reference and (b) CRF configurations

Figures 16a and 16b show the velocity contours over time in the longitudinal median plane presented in Figure 9 during melting respectively for the reference and the CRF configurations.
For the two configurations, at the beginning, the natural convection is negligible. Over time, a fluid movement appears. An asymmetry of the velocity field is visible with high values of velocity magnitude in the bottom region of the PCM indicating vigorous descending flow compared to the upper region. As discussed before, this is the consequence of the density inversion of the PCM (water) at lower temperature range ($0 < T < 4$ °C), where the increase of the liquid PCM density with respect to temperature leads to negative values of the thermal expansion coefficient, otherwise to descending flow in the vicinity of the heating HTF tube.

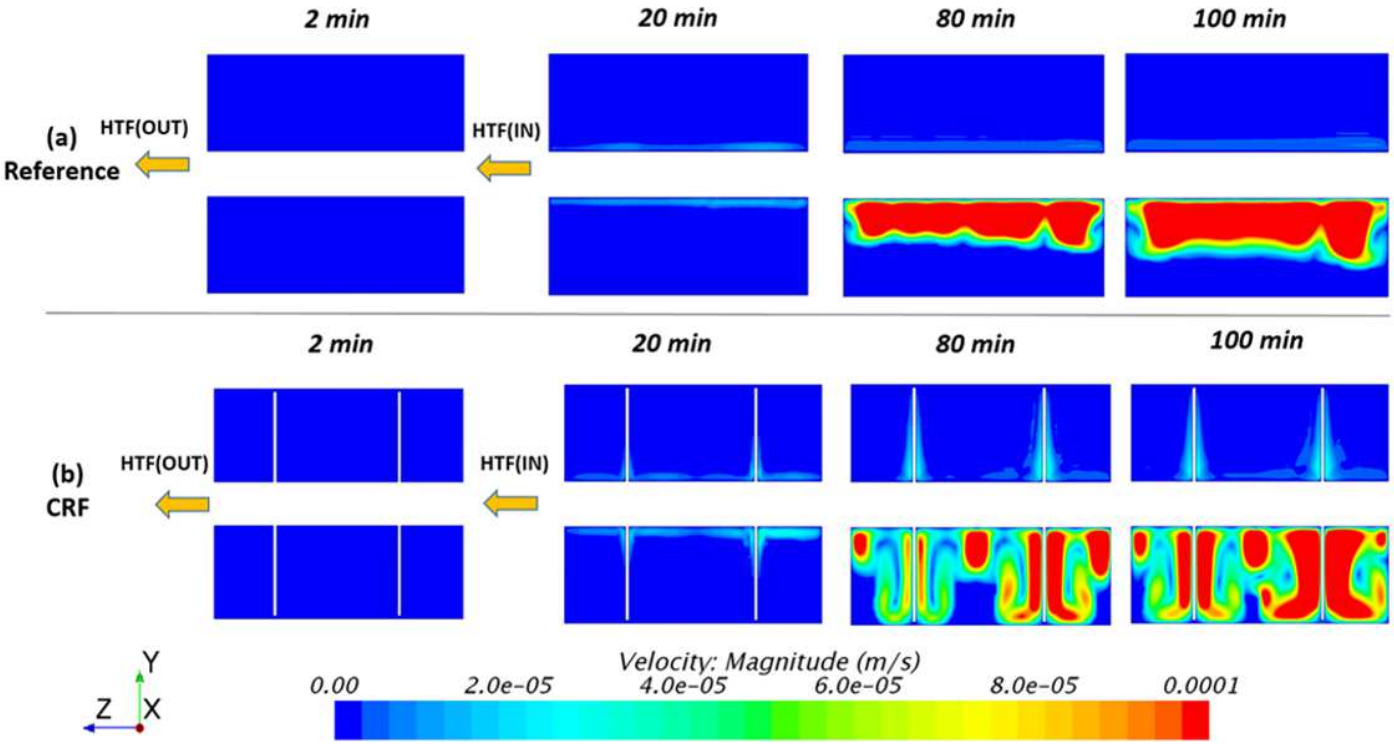

Figure 16 : Illustration of the velocity contours over time in the longitudinal median plane during melting for the (a) reference and (b) CRF configurations

4.2. Global analysis of conducto-convective heat exchanges

4.2.1. Solidification process

In this part, a global analysis of the solidification process during the first two hours of the process is carried out. Figure 17a shows the temporal evolution of the solid volume fraction for the three configurations studied: the reference configuration and the two improved configurations (CRF and CLF). It can be clearly observed that the two configurations with finned tubes have higher kinetics of solidification compared to the reference. The CLF configuration is the most efficient. For this configuration, a solidification rate of approximately 50% is reached in two hours against 43% for the CRF configuration and 27% for the reference configuration. It can be concluded that for the CLF configuration, the performance in terms of kinetics of solidification can almost be doubled compared to the reference. For the two finned tube configurations, the CLF configuration is more efficient although the fact that CLF and CRF configurations have the same heat exchange surface between the HTF and the PCM, and have the same PCM volume.

The same conclusion can be drawn from Figure 17b showing the temporal evolution of the average PCM temperature for the three configurations studied: the reference configuration and the two improved configurations CRF and CLF. A significant difference between the average PCM temperatures for the improved configurations compared to the reference is observed, reaching almost 1°C at 20 minutes. The differences decrease over time due to the decrease of the temperature gradients in the PCM during the solidification.

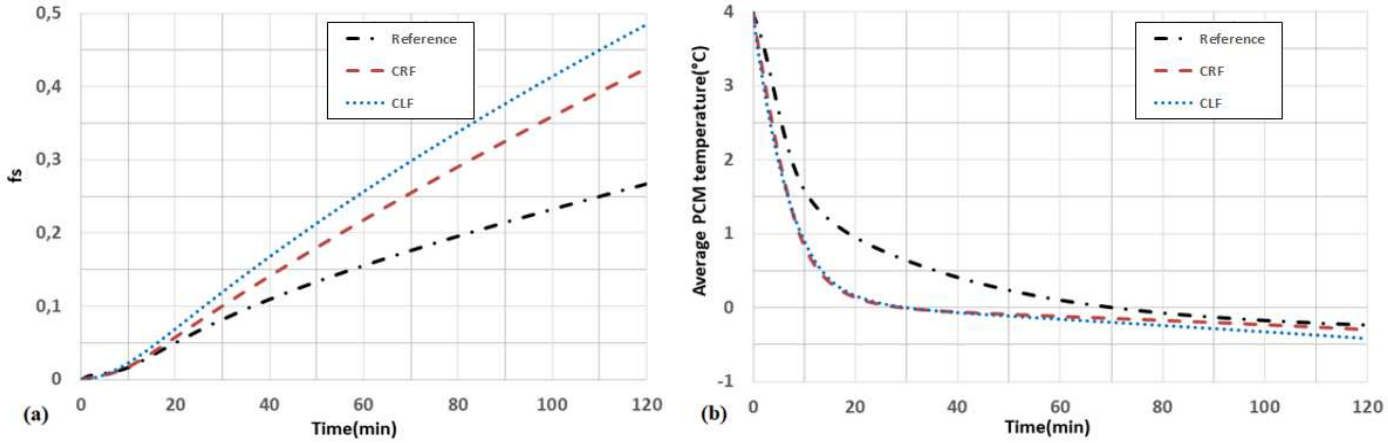

Figure 17 : Temporal evolution of the (a) solid volume fraction and (b) average PCM temperature for the three tested configurations during solidification

In Figure 18, the heat duty exchanged between the PCM and the HTF for the CLF and CRF configurations are compared owing to the fact that they have exactly the same heat exchange surface between the HTF and the PCM.

It can be clearly observed that the heat duty exchanged is more significant for the CLF configuration compared to the CRF configuration at all times. For both configurations, heat duty exchanged reach peak values of almost 20.9 W and 19.5 W respectively for CLF and CRF configurations at the very beginning of the solidification process when the thermal gradients are significant in the PCM. Then, the heat duty exchanged decreases with the decrease of temperature gradients in the PCM.

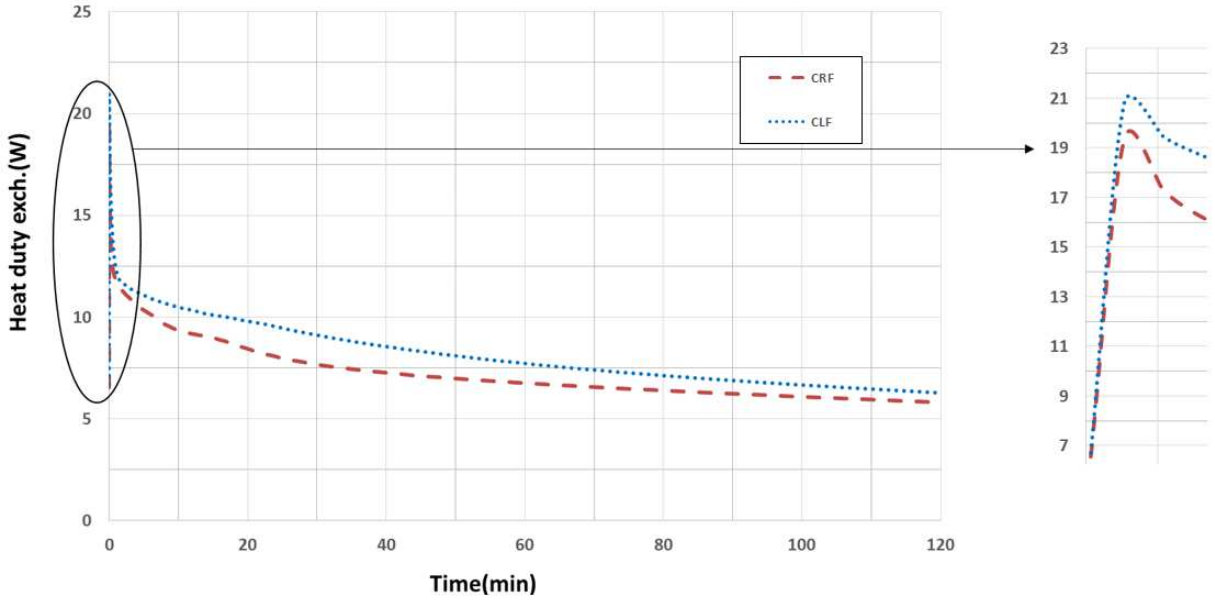

Figure 18 : Temporal evolution of the heat duty exchanged for the CLF and CRF configurations during solidification

4.2.2. Melting process

In this part, a global analysis of the melting process during the first two hours is carried out. Figure 19a shows the temporal evolution of the solid volume fraction for the three configurations studied: the reference configuration and the two improved configurations (CRF and CLF). It can be clearly observed that the two configurations with finned tubes have higher kinetics of melting compared to the reference. The CLF configuration is the most efficient. For this configuration, a melting rate of 50% is reached in two hours against 44% for the CRF configuration and 23% for the reference configuration. It can be concluded that for the CLF configuration, the performance in terms of kinetics of melting can almost be doubled compared to the reference. For the two finned tube configurations, the CLF configuration is more efficient although the fact that the CLF and CRF configurations have the same heat exchange surface between the HTF and the PCM, and have the same PCM volume.

The same conclusion can be drawn from Figure 19b showing the temporal evolution of the average PCM temperature for the three configurations studied: the reference configuration and the two improved configurations CRF and CLF. A significant difference between the average PCM temperatures for the improved configurations compared to the reference is observed, reaching more than 1°C after 10 minutes. The differences decrease over time due to the decrease of the temperature gradients in the PCM.

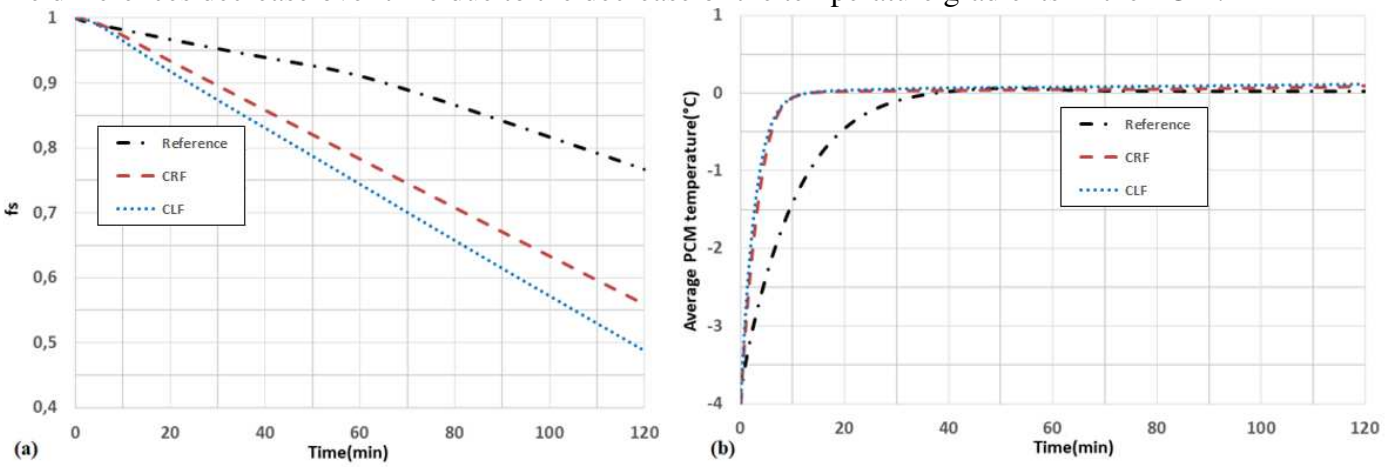

Figure 19 : Temporal evolution of the (a) solid volume fraction and the (b) average PCM temperature for the three tested configurations during melting

In Figure 20, the heat duty exchanged between the PCM and the HTF for the CLF and CRF configurations are compared owing the fact that they have exactly the same heat exchange surface between the HTF and the PCM. It can be clearly observed that the heat duty exchanged is more significant for the CLF configuration compared to the CRF configuration at all times. For both configurations, the heat duty exchanged reach peak values of almost 21.1 W and 19.9 W respectively for CLF and CRF configurations at the very beginning of the melting process when the thermal gradients are significant in the PCM. Then, the heat duty exchanged decreases with the decrease of the temperature gradients in the PCM.

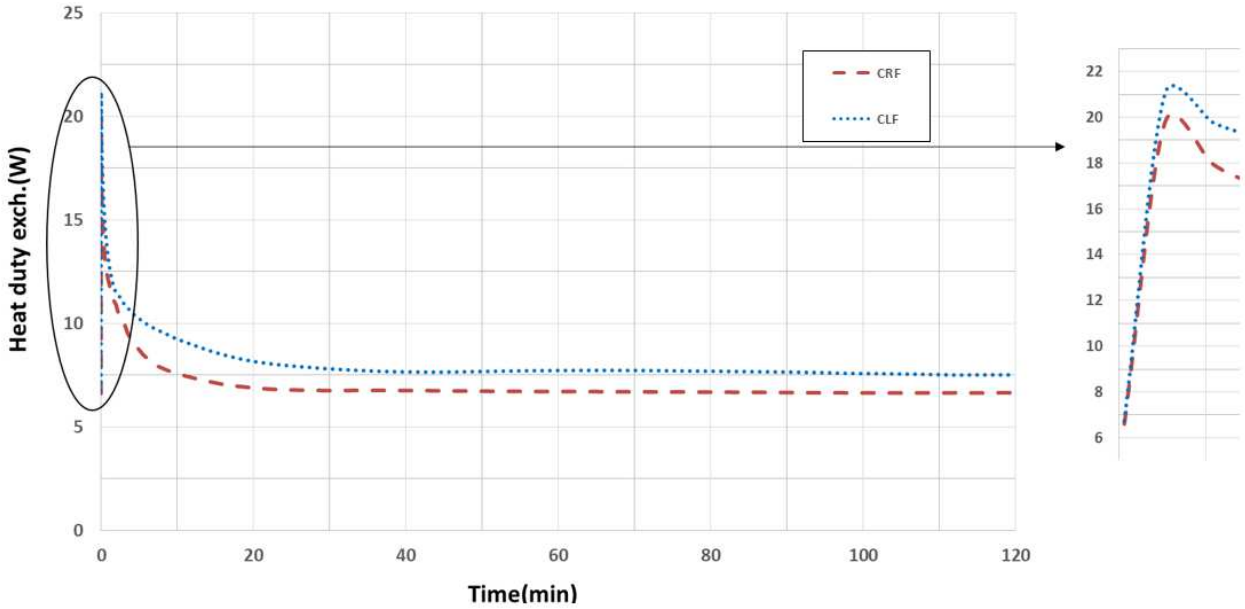

Figure 20 : Temporal evolution of the heat duty exchanged for the CLF and CRF configurations during melting

5. Conclusions

In this study, a three-dimensional numerical analysis of the thermal behaviour of three shell and tube heat exchangers has been carried out under transient state conditions, for low temperature latent heat storage applications (from -4 °C to 4 °C). The basic shell-and-plain tube heat exchanger was used as the reference latent storage unit against which the other two finned tube configurations were compared. The aim of the study was to improve the thermal performance of the reference unit, and therefore to increase the kinetics of

charge and discharge. Effects of surface extension by longitudinal or radial fins on the performance of the two finned-tube units have been studied. The governing equations were solved using the commercial code Star CCM + V12.02. The model developed was dedicated to identify and to quantitatively evaluate the heat storage and the heat transfer performance of LHSU used in agro-food industry.

From this study the main conclusions are the following:

- The addition of longitudinal fins on the tube of a basic shell-and-plain tube storage unit results in a heat transfer intensification that doubles the kinetics of solidification/melting. A solidification rate of approximately 50% is indeed reached for the CLF configuration in two hours against 27% for the reference configuration. A melting rate of 50% is also reached for the CLF configuration in two hours against 23% for the reference configuration.
- For identical shell volume and heat transfer surface, longitudinal added fins provides better heat transfer enhancement and better increase of melting and solidification rates compared to added radial fins. A solidification rate of approximately 50% for the CLF configuration is indeed reached in two hours against 43 % for the CRF configuration. A melting rate of 50% is also reached for the CLF configuration in two hours against 44 % for the CRF configuration.
- The density inversion of the water used as PCM for low temperature applications (from -4 °C to 4 °C) has a significant effect on the flow structure and heat transfer mechanism during melting and solidification.
- Natural convection plays a major role during solidification, especially at the earlier stages of the process, and its effect decreases rapidly over time.
- In contrast to the solidification process, natural convection is quite absent at earlier stages of the melting process and as the time goes, the effect of natural convection becomes significant with increasing volume of melted PCM.

Declaration of Competing Interest

The authors declare that they have no known competing financial interests or personal relationships that could have appeared to influence the work reported in this paper.

Acknowledgements

This study was carried out with the financial support of the Mines Telecom Lille Douai Institute (IMT Lille Douai), the School of Advanced Engineering Studies (HEI-Yncrea-Hauts-de-France) and the Hauts-de-France region via the FEDER-ESF Nord-Pas-de-Calais 2014-2020 grant program to whom we express our sincere thanks.

References

[1]M.A. Dekhil, J.V. Simo Tala, O. Bulliard-Sauret, D. Bougeard, Development of an innovative heat exchanger for sensible heat storage in agro-food industry, Applied Thermal Engineering, 2020.

[2]D. Lafri, D. Semmar, A. Hamid, M. Ouzzane, Experimental investigation on combined sensible and latent heat storage in two different configurations of tank filled with PCM, Applied Thermal Engineering, 2019.

[3]M. Chandrashekara, A. Yadav, An experimental study of the effect of exfoliated graphite solar coating with a sensible heat storage and Scheffler dish for desalination, Applied Thermal Engineering, 2017.

[4]L. Geissbühler, M. Kolman, G. Zanganeh, A. Haselbacher, A. Steinfeld, Analysis of industrial-scale high-temperature combined sensible/latent thermal energy storage, Applied Thermal Engineering, 2016.

[5]K.A.R. Ismaila, R. Stuginsky Jra, A parametric study on possible fixed bed models for pcm and sensible heat storage, Applied Thermal Engineering, 1999.

[6]S. Kunkel, T. Teumer, P. Dörnhofer, K. Schlachter, Y. Weldeslasie, M. Kühr, M. Rädle, J. Repke, Determination of heat transfer coefficients in direct contact latent heat storage systems, Applied Thermal Engineering, 2018.

[7]D. Maderić, B. Pavković, K. Lenić, An experimental research on energy efficiency of a beverage cooler with the latent heat storage, Applied Thermal Engineering, 2019.

[8]R. Abdulrahman, F. Ibrahim, S. Dakhil, Development of paraffin wax as phase change material based latent heat storage in heat exchanger, Applied Thermal Engineering, 2019.

[9]M. Kabbara, D. Groulx, A. Joseph, Experimental investigations of a latent heat energy storage unit using finned tubes, Applied Thermal Engineering, 2016.
[10]M. Kubota, S. Matsumoto, H. Matsuda, Enhancement of hydration rate of LiOH by combining with mesoporous carbon for Low-temperature chemical heat storage, Applied Thermal Engineering, 2019.
[11]O. Myagmarjav, M. Zamengo, J. Ryu, Y. Kato, Energy density enhancement of chemical heat storage material for magnesium oxide/water chemical heat pump, Applied Thermal Engineering, 2015.
[12]O. Myagmarjav, J. Ryu, Y. Kato, Lithium bromide-mediated reaction performance enhancement of a chemical heat-storage material for magnesium oxide/water chemical heat pumps, Applied Thermal Engineering, 2014.
[13]F. Agyenim, N. Hewitt, P. Eames, M. Smyth, A review of materials, heat transfer and phase change problem formulation for latent heat thermal energy storage systems (LHTESS), Renewable and Sustainable Energy Reviews, 2010.
[14]S. Jegadheeswaran, D. Pohekar, Performance enhancement in latent heat thermal storage system: A review, Renewable and Sustainable Energy Reviews, 2009.
[15]E.M. Sparrow, E.D. Larsen, J.W. Ramsey, Freezing on a finned tube for either conduction controlled or natural-convection-controlled heat transfer, Int. J. Heat Mass Transfer, 1981.
[16]P.V. Padmanabhan, M.V. Krishna Murthy, Outward phase change in a cylindrical annulus with axial fins on the inner tube, Int. J. Heat Mass Transfer, 1986.
[17]R. Velraj, R.V. Seeniraj, B. Hafner, C. Faber, K. Schwarzer, Experimental analysis and numerical modelling of inward solidification on a finned vertical tube for a latent heat storage unit, Solar Energy, 1997.
[18]J. Wang, Y. Ouyang, G. Chen, Experimental study on charging processes of a cylindrical heat storage capsule employing multiple-phase-change materials, International Journal of Energy Research, 2001.
[19]J. Wang, G. Chen, F. Zheng, Study on phase change temperature distributions of composite PCMS in thermal energy storage systems, International Journal of Energy Research, 1999.
[20]O. Mesalhy, K. Lafdi, A. Elgafi, K. Bowman, Numerical study for enhancing the thermal conductivity of phase change material (PCM) storage using high thermal conductivity porous matrix, Energy Conversion and Management, 2005.
[21]E.S. Mettawee, G.M.R. Assassa, Thermal conductivity enhancement in a latent heat storage system, Solar Energy, 2007.
[22]H. Ettouney, I. Alatiqi, M. Al-Sahali, K. Al-Hajirie, Heat transfer enhancement in energy storage in spherical capsules filled with paraffin wax and beads, Energy Conversion and Management, 2006.
[23]M.N.A. Hawlader, M.S. Uddin, M.M. Khin, Microencapsulated PCM thermal-energy storage system, Applied Energy, 2003.
[24]B. Chen, X. Wang, R. Zeng, Y. Zhang, X. Wang, J. Niu, Y. Li, H. Di, An experimental study of convective heat transfer with microencapsulated phase change material suspension: laminar flow in a circular tube under constant heat flux, Experimental Thermal and Fluid Science, 2008.
[25]C. Alkan, A. Sari, A. Karaipekli, O. Uzun, Preparation, characterization, and thermal properties of microencapsulated phase change material for thermal energy storage, Solar Energy Materials and Solar Cells, 2009.
[26]H. Inaba, Y. Zhang, A. Horibe, Transient heat storage characteristics on horizontal rectangular enclosures filled with fluidity slurry of micro-encapsulated phase-change-material dispersed in water, Journal of Thermal Science and Technology, 2006.
[27]L.F. Cabeza, H. Mehling, S. Hiebler, F. Ziegler, Heat transfer enhancement in water when used as PCM in thermal energy storage, Applied Thermal Engineering, 2002.
[28]T.J. Scanlon, M.T. Stickland, An experimental and numerical investigation of natural convection melting, International Communications in Heat and Mass Transfer, 2001.
[29]I.W. Eames, K.T. Adref, Freezing and melting of water in spherical enclosures of the type used in thermal (ice) storage systems, Applied Thermal Engineering, 2002.
[30]J. Gasia, N.H. Steven Tay, M. Belusko, L.F. Cabeza, F. Bruno, Experimental investigation of the effect of dynamic melting in a cylindrical shell-and-tube heat exchanger using water as PCM, Applied energy, 2017.
[31]P. Lamberg, R. Lehtiniemi, AM. Henell, Numerical and experimental investigation of melting and freezing processes in phase change material storage, International Journal of Thermal Sciences 2004.
[32]KS. Reddy, Thermal modeling of PCM-based solar integrated collector storage water heating system, Journal of Solar Energy Engineering, 2007.
[33]M. Faden, C. Linhardt, S. Höhlein, A. König-Haagen, D. Brüggemann, Velocity field and phase boundary measurements during melting of n-octadecane in a cubical test cell, International Journal of Heat and Mass Transfer, 2019.
[34]S. Jevnikar, K. Siddiqui, Investigation of the influence of heat source orientation on the transient flow behavior during PCM melting using particle image velocimetry, Journal of Energy Storage, 2019.

[35]E. Assis, L. Katsman, G. Ziskind , R. Letan, Numerical and experimental study of melting in a spherical shell, International Journal of Heat and Mass Transfer, 2006.
[36]M. Lacroix, Study of the heat transfer behavior of a latent heat thermal energy storage unit with a finned tube, International Journal of Heat and Mass Transfer, 1992.
[37]M.Y. Yazici, M. Avci, O. Aydin, M. Akgun, Effect of eccentricity on melting behavior of paraffin in a horizontal tube-in-shell storage unit: An experimental study, solar energy, 2014.
[38]M.J. Hosseini, A.A. Ranjbar, K. Sedighi, M. Rahimi, A combined experimental and computational study on the melting behavior of a medium temperature phase change storage material inside shell and tube heat exchanger, International Communications in Heat and Mass Transfer, 2012.
[39]M. Longeon, A. Soupart, J-F. Fourmigué, A. Bruch, P. Marty, Experimental and numerical study of annular PCM storage in the presence of natural convection, Applied energy, 2013.
[40]G.S. Sodhi, A.K. Jaiswal, K. Vigneshwaran, P. Muthukumar, Investigation of charging and discharging characteristics of a horizontal conical shell and tube latent thermal energy storage device, Energy Conversion and Management, 2019.
[41]H. Niyas, S. Prasad, P. Muthukumar, Performance investigation of a lab–scale latent heat storage prototype – Numerical results, energy conversion and management, 2017.
[42]R.V. Seeniraj, R. Velraj, N.L. Narasimhan, Thermal analysis of a finned-tube LHTS module for a solar dynamic power system, Heat and Mass Transfer, 2002.
[43]CD-Adapco. Starccm+ v12.02 user guide. User guide, 2017.
[44]D. Bohne, S. Fischer, E. Obermeier, Thermal Conductivity, Density, Viscosity, and Prandtl-Numbers of Ethylene Glycol-Water Mixtures, Physical Chemistry Chemical Physics, 1984.
[45]https://www.engineeringtoolbox.com/material-properties-t_24.html
[46]Y. C. Yen, Review of thermal properties of snow, ice and sea ice / by Yin-Chao Yen. Hanover, N.H.: U.S. Cold Regions Research and Engineering Laboratory; Springfield, Va.: available from National Technical Information Service, 1981.
[47]J. H. Lienhard IV, J. H. Lienhard V, A heat transfer textbook, Fourth edition, 2017.
[48]N. Hannoun, V. Alexiades, T.Z. Mai, A reference solution for phase change with convection, International journal for numerical methods in fluids, 2005.
[49]P. Lamberg, Approximate analytical model for two-phase solidification problem in a finned phase-change material storage, Applied Energy, 2004.
[50]U. Stritih, An experimental study of enhanced heat transfer in rectangular PCM storage, International Journal of Heat and Mass Transfer, 2004.
[51]P. Lamberg, K. Siren, Analytical model for melting in a semi-infinite PCM storage with an internal fin, Heat and Mass Transfer, 2003.